Supplementary Information

Decoupling charge–discharge electrolysis for accelerating hydrogen evolution and organic oxidation reactions

Huang et al.

Supplementary Table 1 Theoretical oxidation potential and transferred electron numbers of OORs.

	Reactants	Products	TOP[a] (V vs. RHE)	TEN[b]
Alcohols	Methanol	Formic acid	1.33[1]	4
	Ethanol	Formic acid	1.3[2]	8
		Acetic acid	0.754[3]	4
	Ethylene glycol	Formic acid	1.25[4]	6
		Alycolic acid	0.57[5]	4
	Glycerol	Formic acid	1.42[6]	8
		Lactic acid	0.9[7]	2
	Benzyl alcohol	benzaldehyde	0.43[8]	2
		Benzoic acid	1.3[9]	4
Aldehydes	Formaldehyde	Formic acid	-0.13[10]	2
	2-Furaldehyde	2-Furoic acid	1.45[11]	2
	5-Hydroxymethylfurfural	2,5-furandicarboxylic acid	1.25[12]	6
Amines	Benzylamine	Benzonitrile	1.37[13]	4
	Tetrahydroisoquinolines	Dihydroisoquinolines	1.35[14]	2
	Urea	N_2 and CO_2	0.325[15]	6
	Propylamine	Propionitrile	1.32[16]	4
Polyalcohols	Glucose	Glucaric acid	1.2[17]	2
		Lactic acid	1.3[18]	4
	Ascorbic acid	Dehydroascorbic acid	0.45[19]	2

[a] Theoretical oxidation potential (TOP), [b] Transferred electron numbers (TEN)

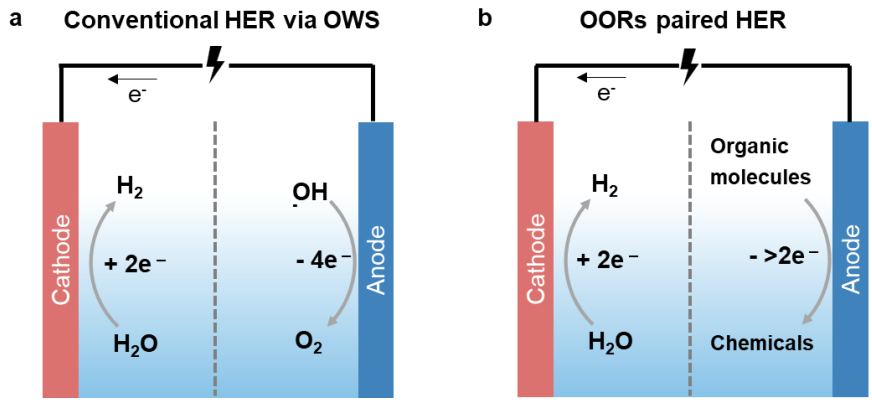

Supplementary Fig. 1 Schematic of the operation mechanism of the (a) conventionally configured OWS and (b) ORRs-paired HER systems.

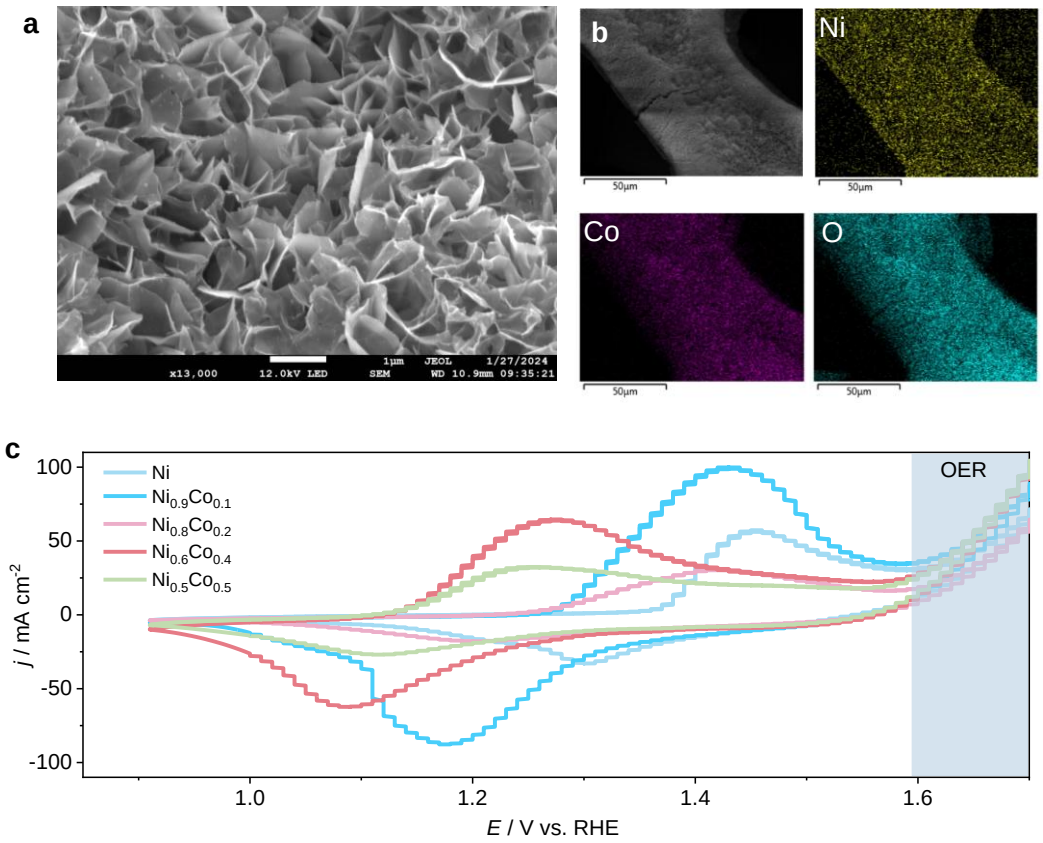

Supplementary Fig. 2 (a) SEM and (b) EDX elemental mapping images of NCOH. (**c**) CV curves of $Ni_{1-x}Co_x(OH)_2$ with different Ni/Co ratios.

Supplementary Note 1 SEM and elemental mapping images in Supplementary Fig. 2a,b show the nanosheet array structure of NCOH and highly dispersed Co and Ni species. The redox potential of $Ni(OH)_2$/NiOOH decreased with increasing Co addition (Supplementary Fig. 2c), which can prevent competition with the OER during the charging of NCOH.[20] Here, $Ni_{0.6}Ni_{0.4}(OH)_2$ (named NCOH in the manuscript), with a Ni/Co mole ratio of 3/2, was selected as the optimal RM electrode.

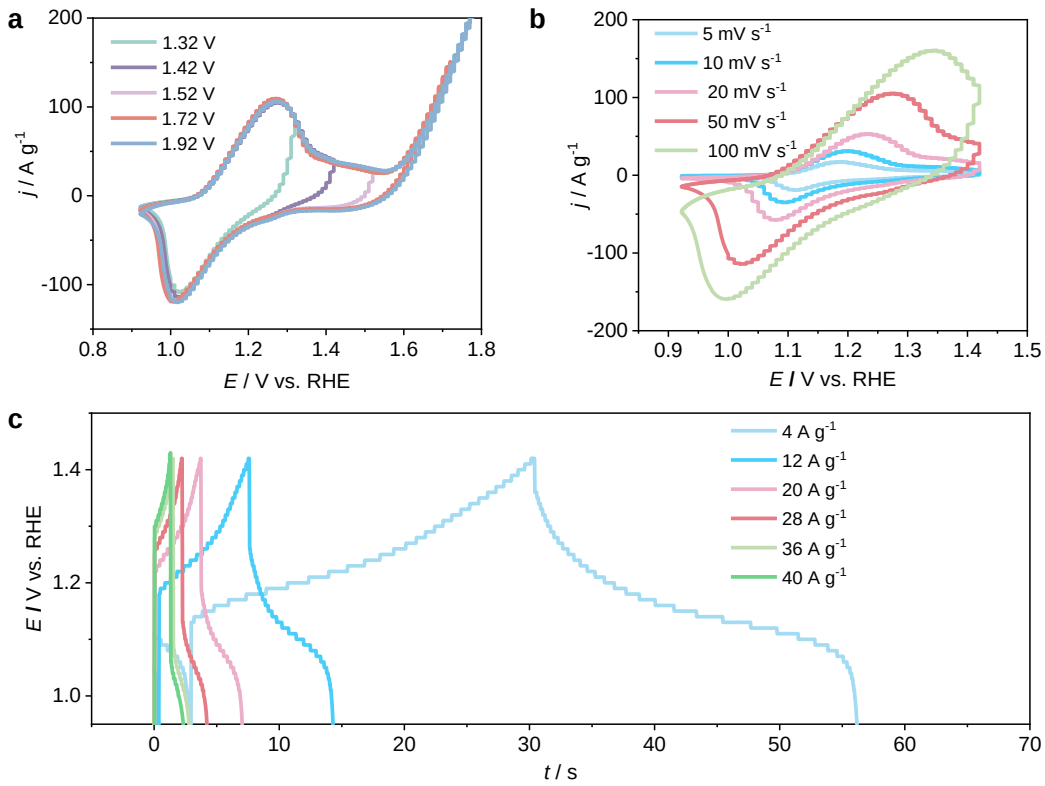

Supplementary Fig. 3 (a) CV curves of NCOH under different voltage ranges at a sweep rate of 50 mV s^{-1}. (b) CV curves of NCOH at different sweep rates. (c) Galvanostatic charge-discharge (GCD) curves of NCOH at different current densities in a 1 M KOH electrolyte.

Supplementary Note 2 Supplementary Fig. 3a shows that the material exhibits negligible polarization when the CV potential window was set to 0.9–1.4 V (vs. RHE). Supplementary Fig. 3b shows that the shape of the CV curve exhibited minimal distortion with increasing scan rates at a high scan rate of 50 mV s^{-1}, suggesting rapid electron transfer kinetics, which indicates that NCOH has excellent reversibility. The GCD curves of NCOH at different current densities from 4 A g^{-1} to 40 A g^{-1} are shown in supplementary Fig. 3c. NCOH clearly has ultrahigh specific capacitances of 220 C g^{-1} and 168 C g^{-1} at current densities of 4 and 12 A g^{-1}, respectively. At a strong current density of 40 A g^{-1}, the specific capacitance of 96 C g^{-1} can still be retained, indicating outstanding electrochemical reversibility.

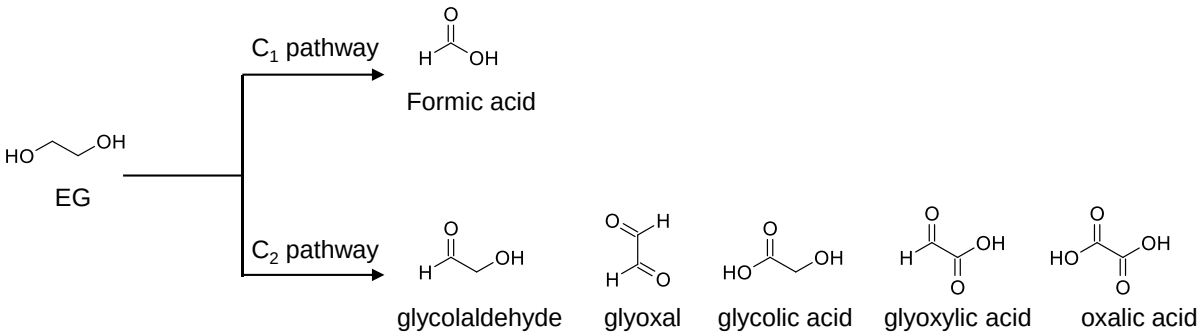

Supplementary Fig. 4 Proposed reaction mechanisms for the electrooxidation of EG to C2 and C1 chemicals.

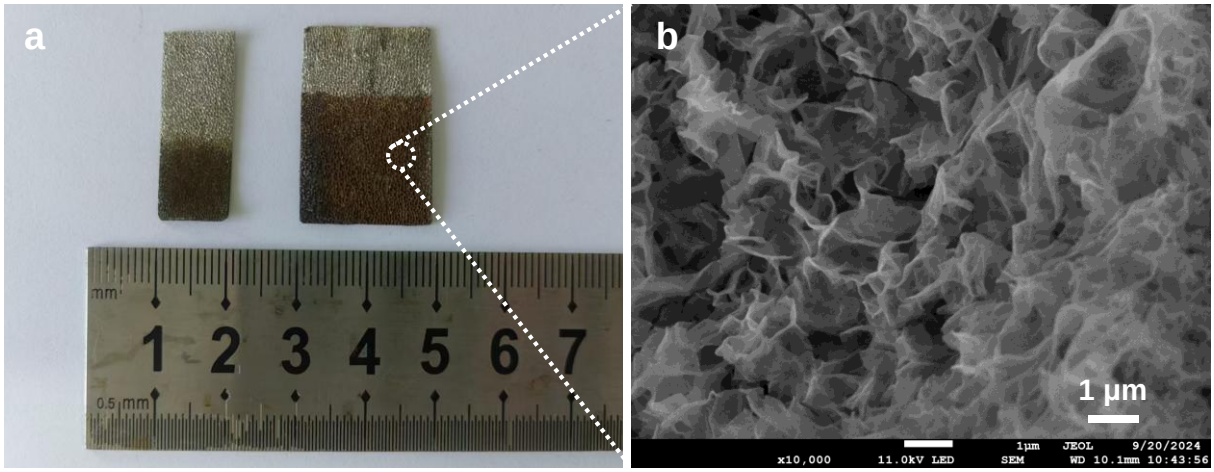

Supplementary Fig. 5 (a) Optical photo and (b) SEM image of Pd PNAs.

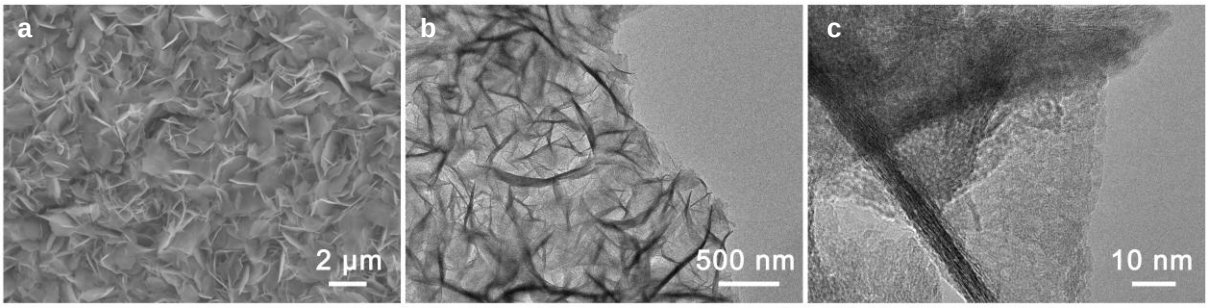

Supplementary Fig. 6 (a) SEM and (b) TEM images of $Co(OH)_2$ nanosheet arrays.

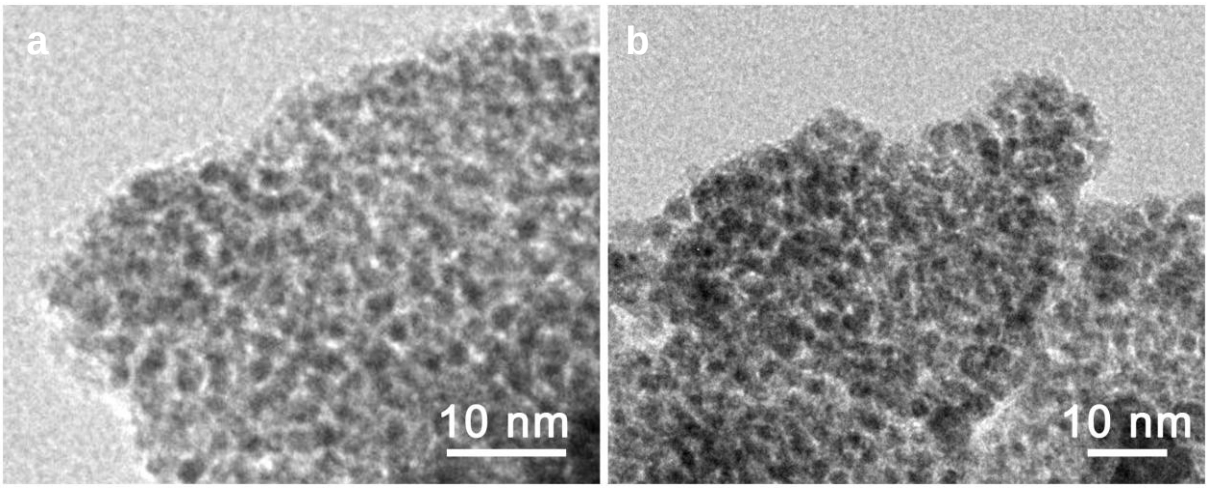

Supplementary Fig. 7 TEM images of Pd PNAs.

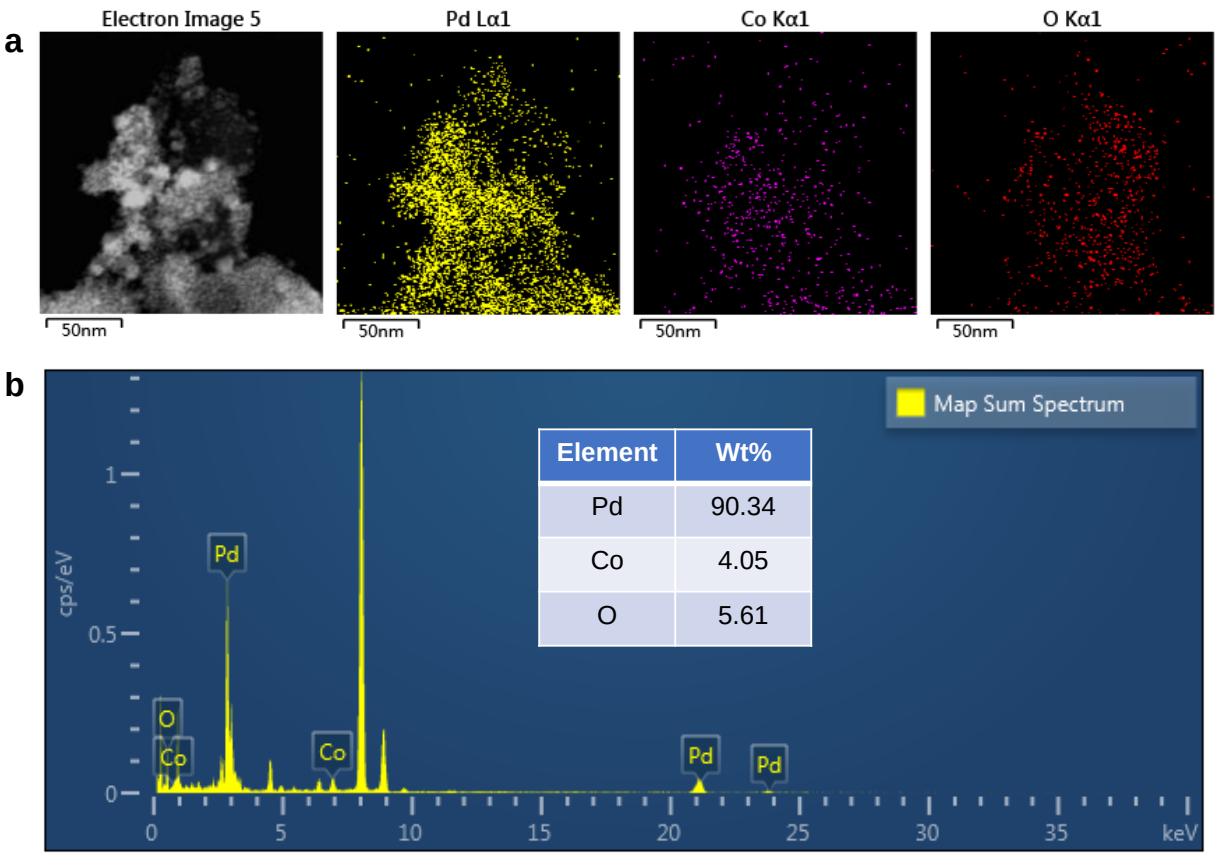

Supplementary Fig. 8 (a) High-angle annular dark-field scanning transmission electron microscopy (HAADF-STEM) and element mapping images of Pd PNAs. (b) EDS spectrum of Pd PNAs.

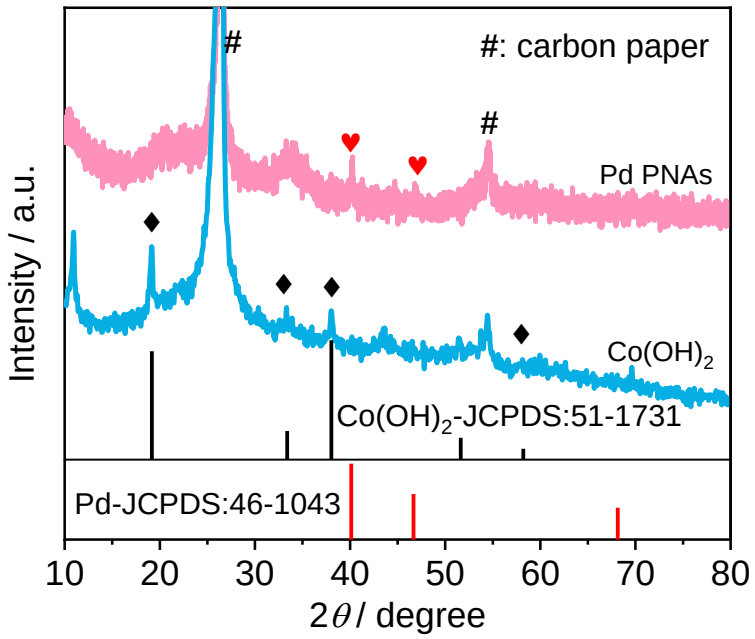

Supplementary Fig. 9 XRD patterns of $Co(OH)_2$ and Pd PNAs.

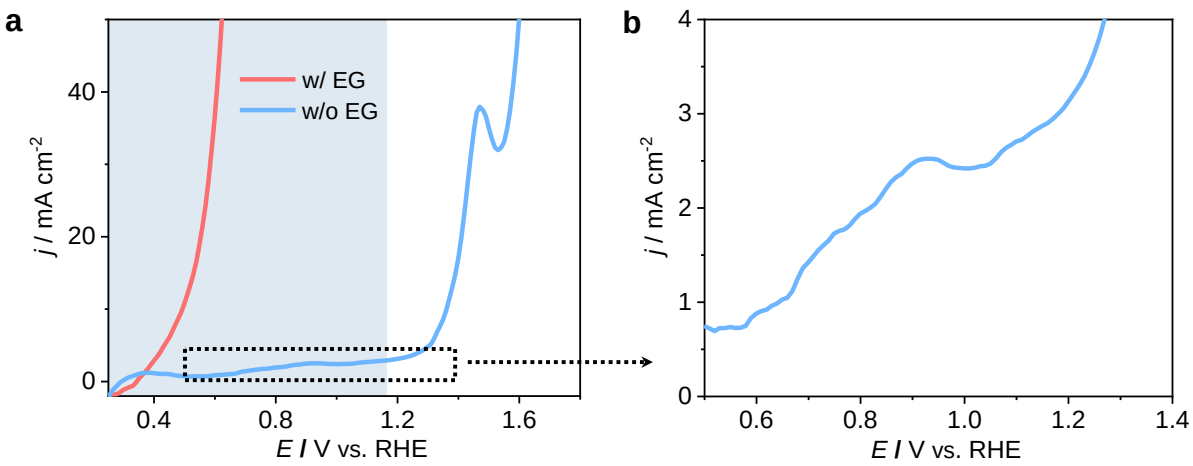

Supplementary Fig. 10 (a, b) Linear sweep voltammetry (LSV) curves of Pd PNAs in the presence (red line) and absence (blue line) of EG.

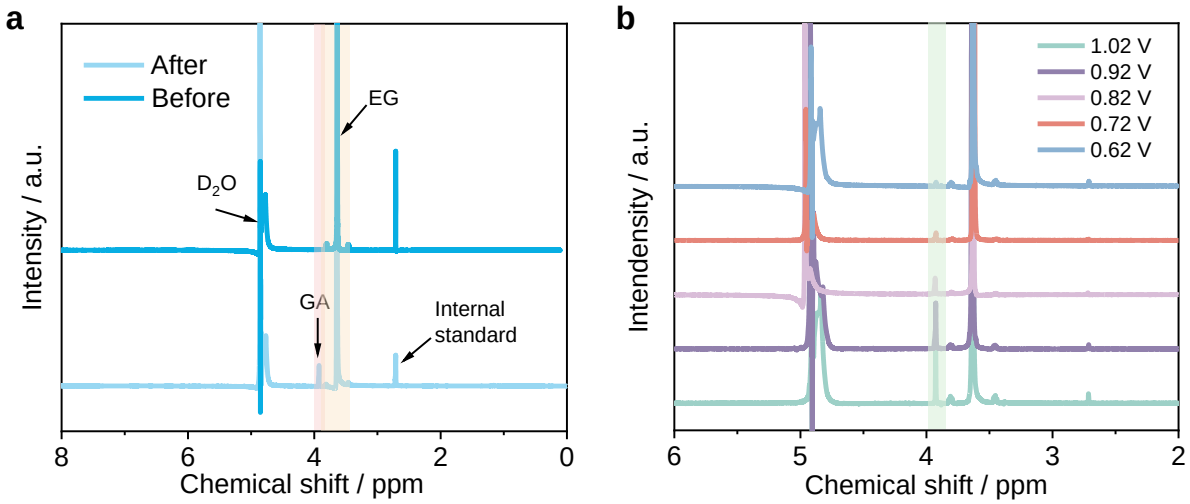

Supplementary Fig. 11 (**a**) ^{1}H nuclear magnetic resonance (NMR) spectra of GA generated from Pd PNAs and standard GA solutions. (**b**) ^{1}H NMR spectra of GA generated from Pd PNAs under various applied potentials. Dimethyl sulfoxide (DMSO) was used as the internal standard.

Supplementary Table 2 Comparison of recently reported EGOR electrocatalysts.

Catalysts	Conditions	Products	Potential	FE_{GA}	Ref
$Pd/NiMoO_4/NF$	1.0 M NaOH + 1 M EG	GA	0.79 V vs. RHE (j = 100 mA cm^{-2})	95.7%	[21]
$Pt–Ni(OH)_2/NF$	1.0 M KOH + 0.1 M EG	GA	0.69 V vs. RHE (j = 100 mA cm^{-2})	93%	[22]
Pd NTs/NF	1.0 M KOH	GA	~0.7 V vs. RHE[a] (j = 100 mA cm^{-2})	~87%	[23]
PdAg/NF	0.5 M KOH + 1 M EG	GA	~0.9 V vs. RHE[a] (j = 100 mA cm^{-2})	92%	[24]
Pt/γ-NiOOH/NF	1.0 M KOH + 0.3 M EG	GA	~0.6 V vs. RHE[a] (j = 100 mA cm^{-2})	97%	[25]
$Pd–Ni(OH)_2/NF$	1.0 M KOH + 1.0 M EG	GA	0.69 V vs. RHE (j = 100 mA cm^{-2}) ~1.2 V vs. RHE (j = 600 mA cm^{-2})	94.1%	[26]
$Au/Ni(OH)_2$	3.0 M KOH + 0.3 M EG	GA	1.0 V vs. RHE[a] (j = 100 mA cm^{-2}) 1.35 V vs. RHE (j = 609.9 mA cm^{-2})	~	[27]
$Cu_{30}Pd_{70}/NF$	1.0 M KOH + 0.5 M EG	GA	~0.7 V vs. RHE[a] (j = 100 mA cm^{-2})	89%	[28]
$Pd\text{-}CuCo_2O_4$	1 M NaOH + 0.5 M NaCl + 1 M EG	GA	0.8 V vs. RHE[a] (j = 200 mA cm^{-2}) 1.15 V vs. RHE (j = 600 mA cm^{-2})	90.1%	[29]
Pd PNAs	**1.0 M KOH + 0.5 M EG**	**GA**	**0.67 V vs. RHE (j = 100 mA cm^{-2}) 0.75 V vs. RHE (j = 200 mA cm^{-2}) 1.02 V vs. RHE (j = 600 mA cm^{-2})**	**95%**	**This work**

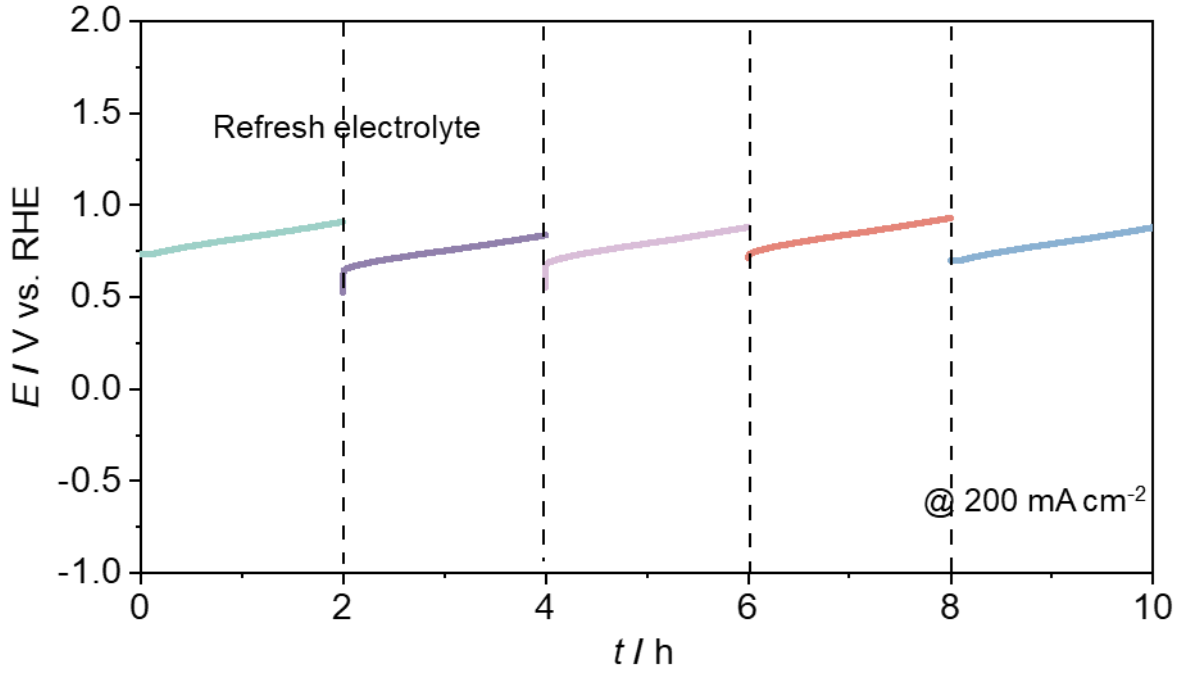

Supplementary Fig. 12 Stability test of Pd PNAs.

.

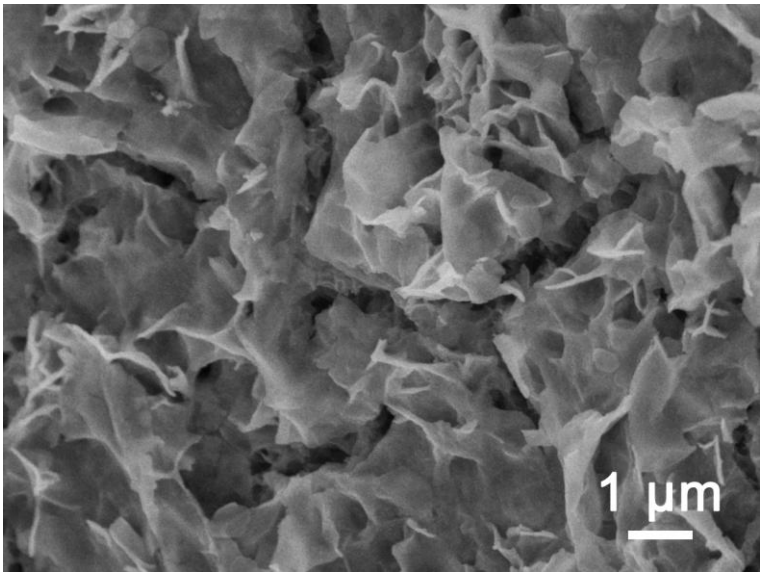

Supplementary Fig. 13 SEM image of Pd PNAs after the stability test.

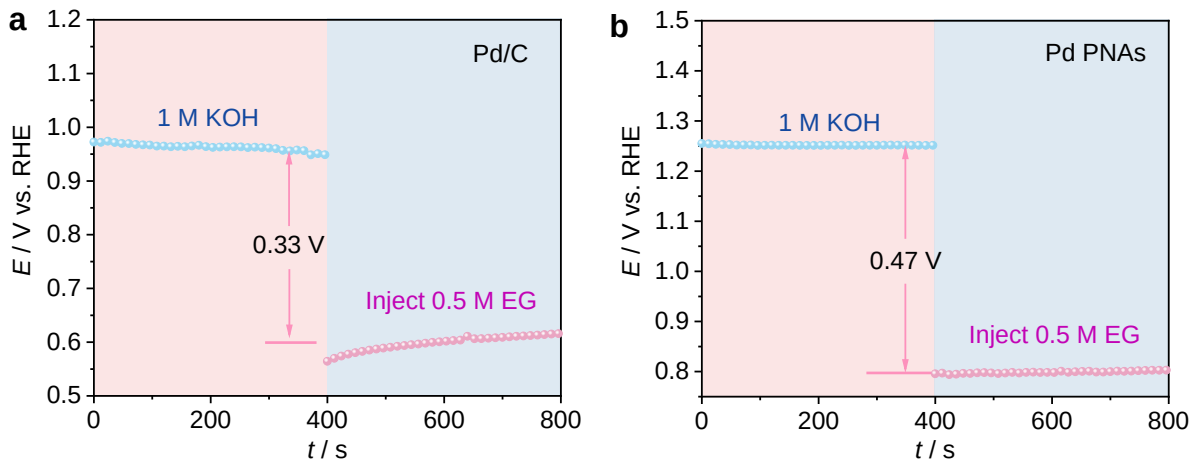

Supplementary Fig. 14 OCP measurements of (a) Pd/C and (b) Pd PNAs upon the addition of 0.5 M EG in 1 M KOH.

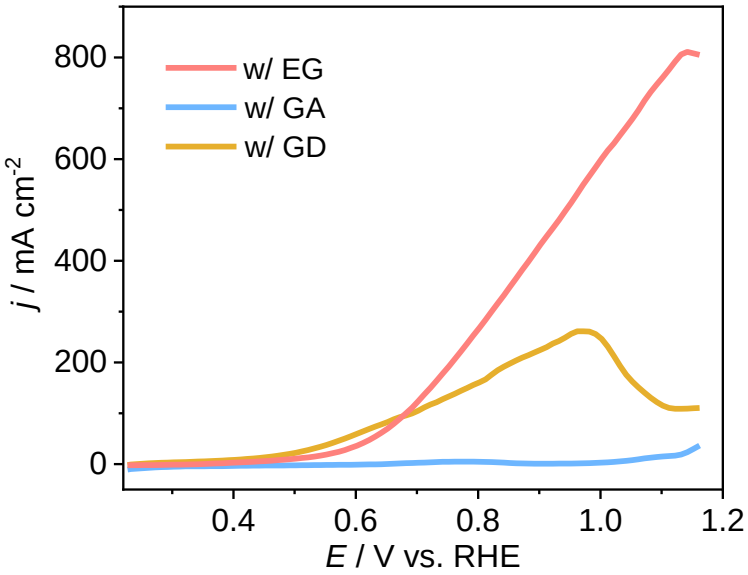

Supplementary Fig. 15 LSV curves of Pd PNAs in the presence of EG, GA and GD.

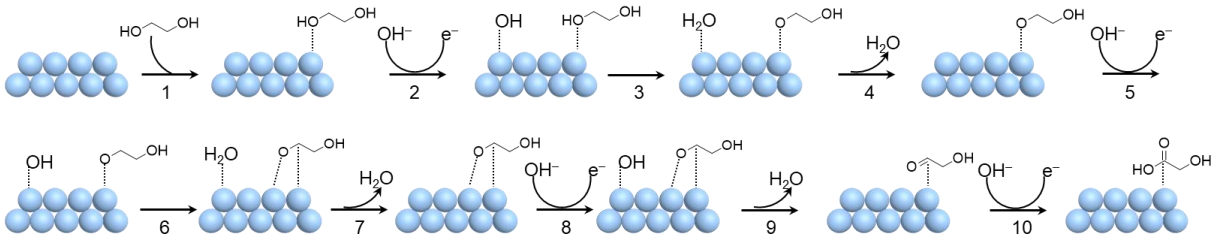

Supplementary Fig. 16 Schematic illustration of the elementary reaction process for the electrooxidation of EG to GA on Pd PANs.

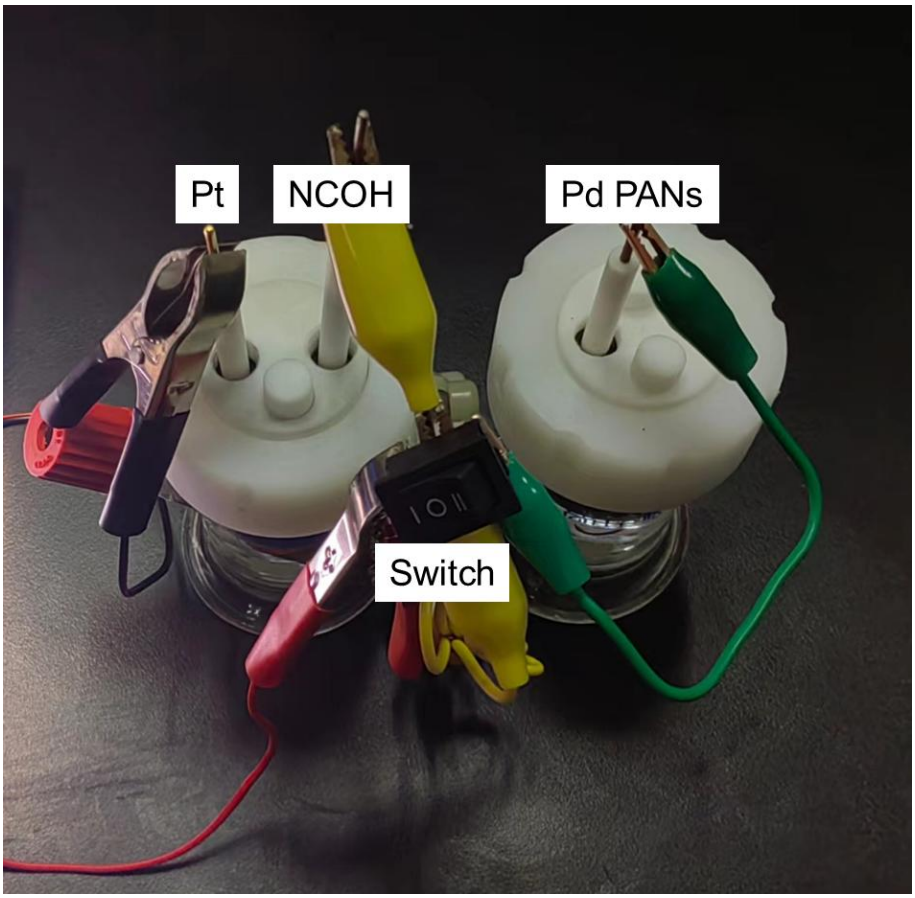

Supplementary Fig. 17 Photograph illustrating the decoupled cell.

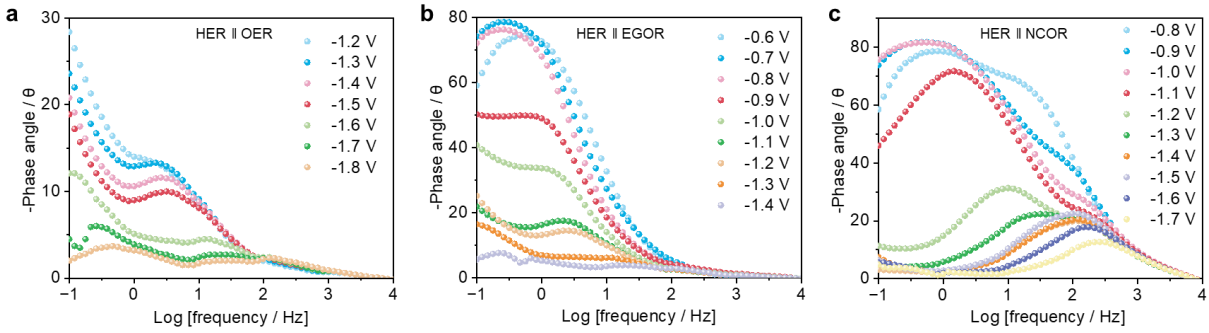

Supplementary Fig. 18 Bode phase plots of (a) HER ‖ OER, (b) HER ‖ EGOR and (**c**) HER ‖ NCOR at various potentials in a 1 M KOH electrolyte.

Supplementary Note 3 The phase angle in supplementary Fig. 18a significantly decreases in the low-frequency region, indicating a progressive shift in the dominant charge transfer mechanism during the reaction. As the potential becomes more negative, the electrode surface provides increased availability of electrons, thereby facilitating redox reactions. This change directly impacts the reaction kinetics. The phase angle changes from -0.6 V to -1.4 V in supplementary Fig. 18b reveal significant kinetic transformations at the electrode interface, driven by the applied potential. The broader phase angle peak in the mid-frequency region of supplementary Fig. 18c suggests improved synchronization of the Volmer–Heyrovsky steps under NCOR (negative cathodic overpotential region) conditions. The Heyrovsky step (electrochemical desorption) likely dominates, whereas the Tafel step is suppressed, reducing surface H* accumulation and increasing reaction rates. The lower phase angle in the high-frequency region indicates a reduced charge transfer resistance and activation energy for H* adsorption, demonstrating excellent interfacial and catalytic performance under NCOR conditions.

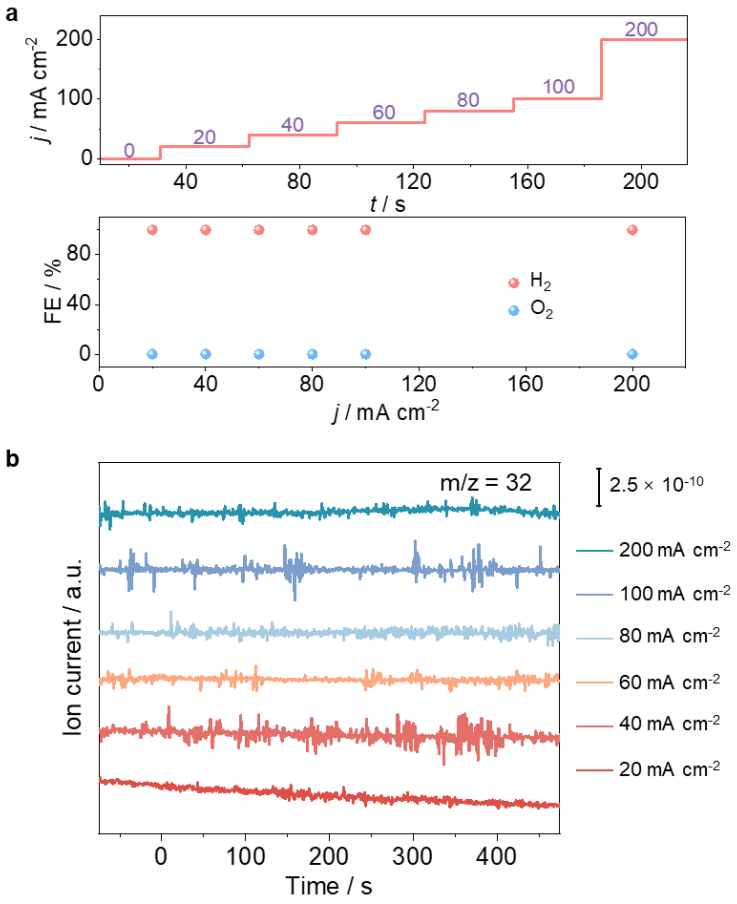

Supplementary Fig. 19 (a) FEs of H_2 and O_2 (b) *Operando* online DEMS curves in Step 1 at different current densities.

Supplementary Note 4 Online gas chromatography (GC) was used to monitor the generated gas in Step 1, and no oxygen was detected at the NCOH anode (Supplementary Fig. 19a). The absence of the OER at the NCOH anode is also supported by *operando* online differential electrochemical mass spectrometry (DEMS) measurements using a scanning flow cell (SFC) in which NCOH was used as the working electrode biased at various constant current densities (see details below). No O_2 signal (m/z = 32) is detected across a current density range of 20 to 200 $mAcm^{-2}$ (Supplementary Fig. 19b).

***Operando* DEMS analysis:** *Operando* online DEMS analysis was conducted with a QAS 100 instrument provided by Linglu Instruments. The flow cell used in the performance evaluation and the DEMS were coupled to ensure that the gas at the flow cell outlet was directly injected into the negatively pressured gas circuit system of the DEMS through a quartz capillary that was inserted into the outlet of the flow cell. A rectangular wave current density was applied from 20 to 200 mA cm^{-2} with a constant interval of 400 s by an electrochemical workstation.

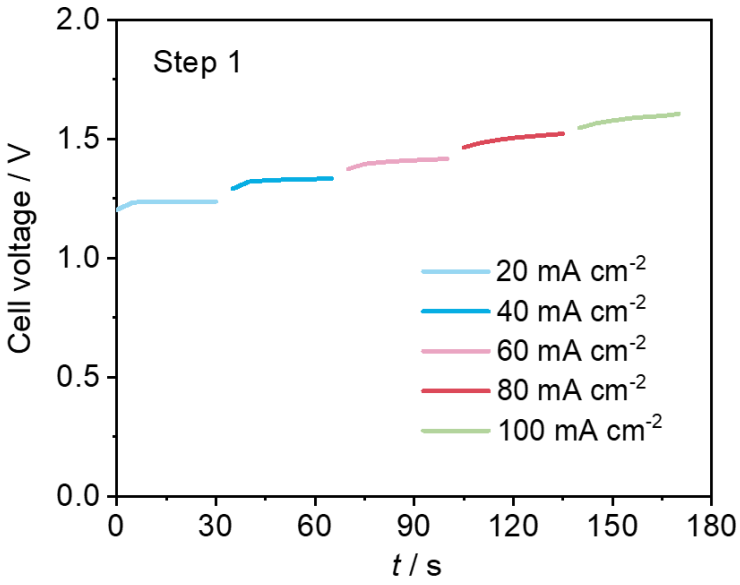

Supplementary Fig. 20 Cell voltage curves of NCOH at different current densities during the charging process.

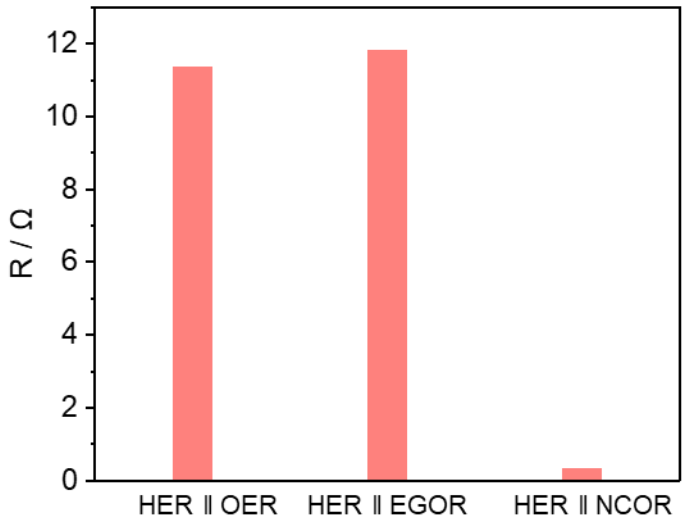

Supplementary Fig. 21. Comparison of the internal resistance of the HER ‖ OER, HER ‖ EGOR and HER ‖ NCOR systems.

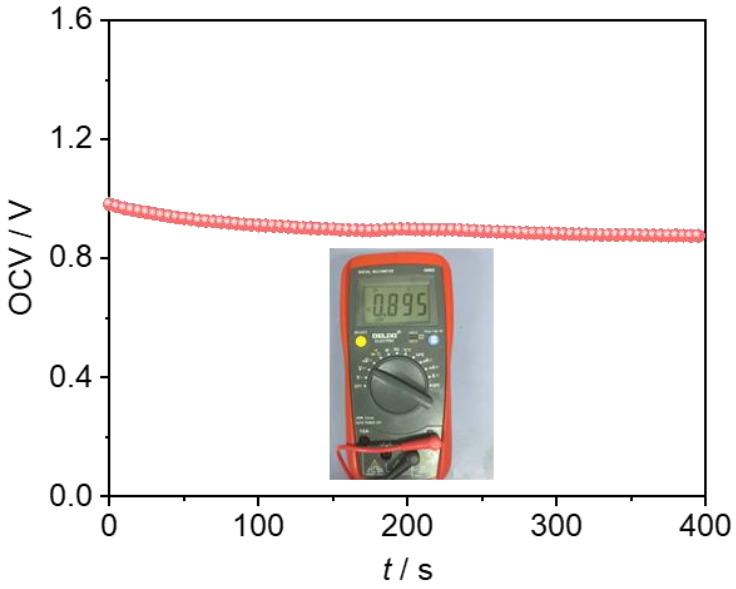

Supplementary Fig. 22 OCV measurement of the battery.

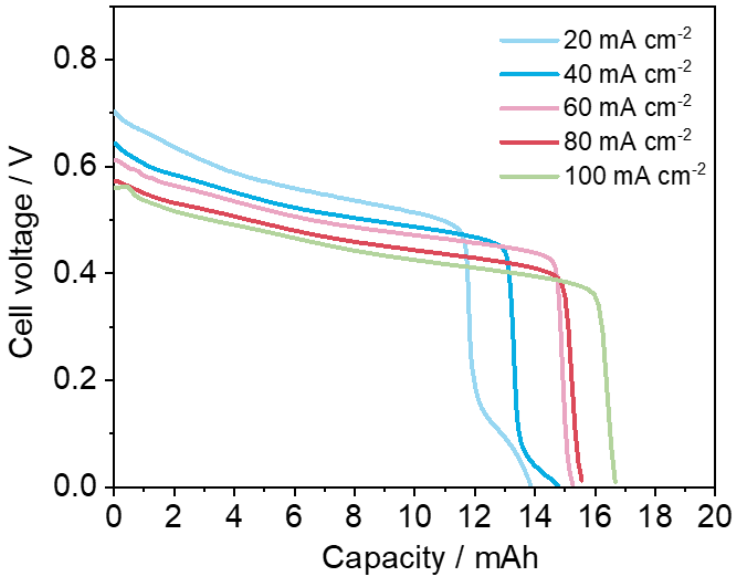

Supplementary Fig. 23 Discharging curves of NCOH in Step 2 at different current densities.

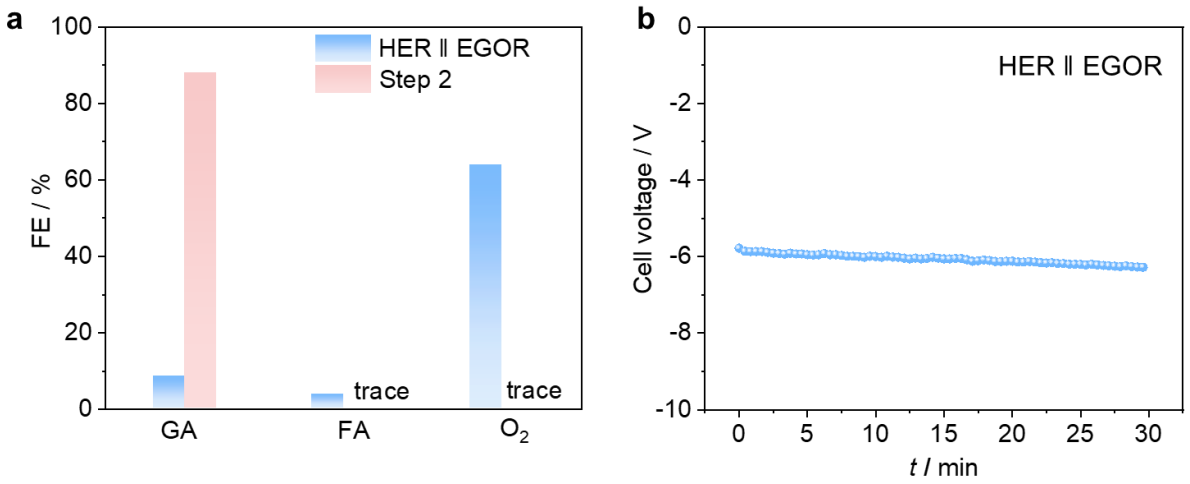

Supplementary Fig. 24 (a) FE of each product (GA, FA and O_2) in the HER ‖ EGOR and Step 2 under a current density of 100 mA cm^{-2}. (b) Cell voltage measurement of HER ‖ EGOR at a current of 100 mA cm^{-2}.

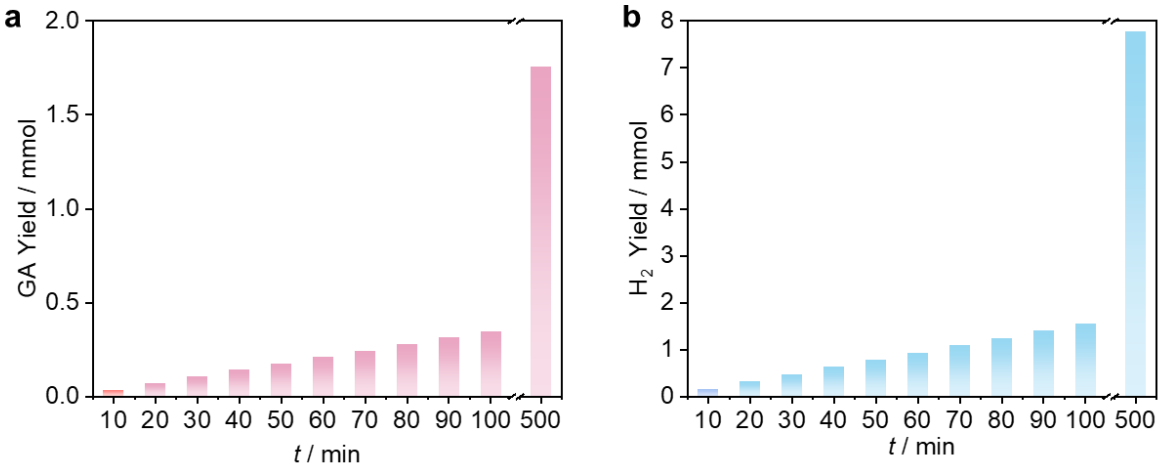

Supplementary Fig. 25 (**a**) Yield of the GA in Step 2 and (**b**) yield of H_2 in Step 1 during 50 full cycles.

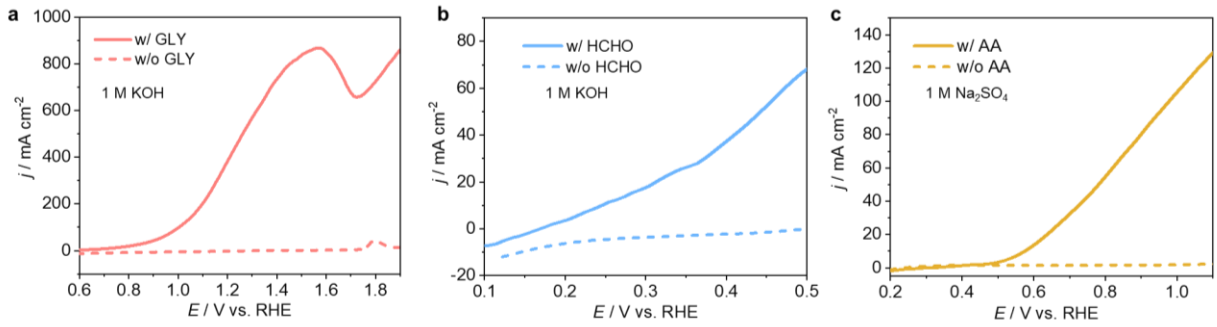

Supplementary Fig. 26 LSV curves of (**a**) GLY oxidation to LA on Au/NF, (**b**) FD oxidation to FA on Cu/CP, and (**c**) AA oxidation to DHA on single-aotm Fe (Fe-SAC).

Supplementary Note 5

Synthesis of Au/NF

First, a piece of Ni foam (0.5 cm ×0.5 cm) was sequentially washed with acetone, ethanol, and deionized water, each for 15 minutes, to ensure thorough removal of contaminants. Then, the cleaned Ni foam was immersed in a 10 mg/mL $NaAuCl_4$ aqueous solution at room temperature for 40 min. The resulting Ni foam was removed, cleaned with deionized water and ethanol several times, and dried in a vacuum oven overnight.

Synthesis of Cu/CP

Cu was electrodeposited on carbon paper (CP) at −0.2 V vs. Ag/AgCl for 900 s in a three-electrode configuration with a Ag/AgCl (saturated KCl) reference electrode and a carbon rod as the counter electrode. The electrolyte was an 8 mM KOH aqueous solution. The prepared Cu was thoroughly rinsed multiple times with deionized water and ethanol to remove residual impurities and subsequently dried in a vacuum oven overnight.

Synthesis of Fe-SAC

Fe-SAC was synthesized according to previous work.[30] First, 13.8 mg of iron(II) acetate and 100.3 mg of 1,10-phenanthroline monohydrate were dissolved in 2 mL of ethanol, followed by stirring for 20 minutes at room temperature. Subsequently, 69.6 mg of carbon black was added to the solution, and the mixture was heated in an oil bath at 60 ℃ under continuous magnetic stirring for 4 hours. The resulting dispersion was then heated at 80 ℃ in air for 12 hours to evaporate the ethanol, yielding a black solid, which was lightly ground using a mortar and pestle. The ground solid was transferred to a ceramic crucible and subjected to thermal treatment in a tube furnace at 600 ℃ under an argon atmosphere (heating rate: 10 ℃/min) for 2 hours. The final product, obtained after cooling to room temperature, was denoted as Fe-SAC.

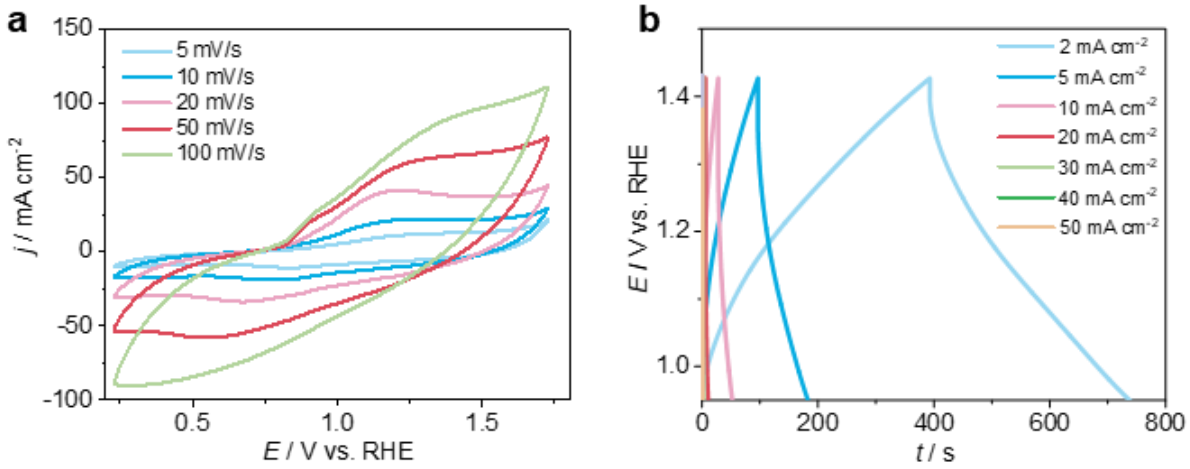

Supplementary Fig. 27 (**a**) CV curves at different sweep rates of $Na_{0.44}MnO_2$ in a 1 M NaOH electrolyte. (**b**) GCD curves of $Na_{0.44}MnO_2$ at different current densities.

Supplementary Note 6 Supplementary Fig. 27a shows increasing current density with increasing scan rates, indicating enhanced charge transfer dynamics and potential contributions from surface-controlled processes. GCD at different current densities (2–50 mA cm^{-2}) in supplementary Fig. 27b shows a gradual increase in overpotential with increasing current density, reflecting the impact of mass transport limitations and reaction kinetics on electrode performance.

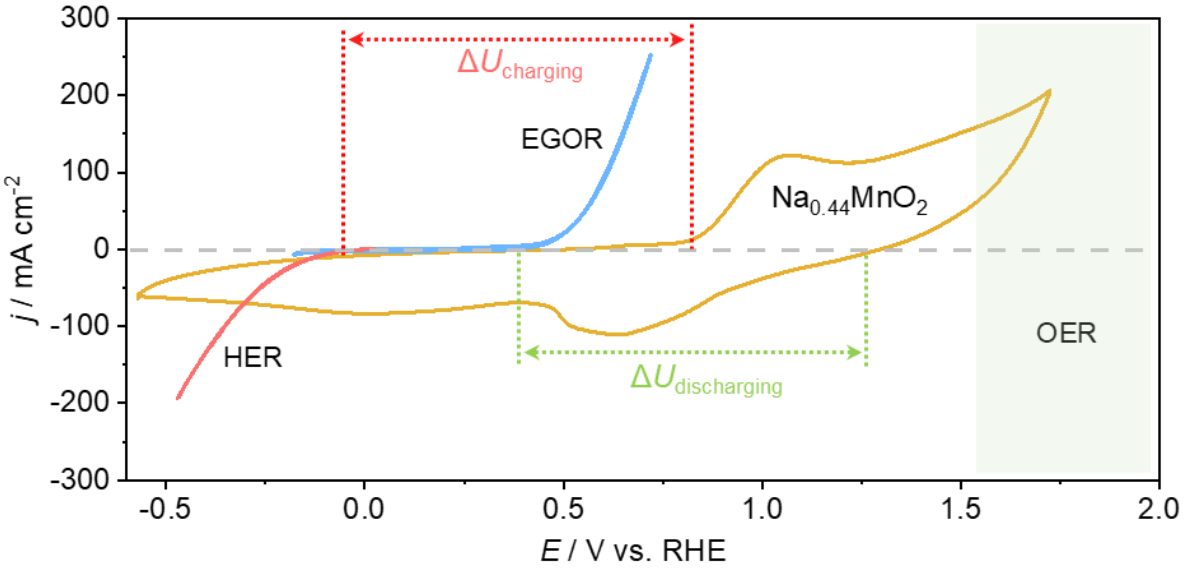

Supplementary Fig. 28 CV curves of the $Na_{0.44}MnO_2$ electrode (yellow line) and LSV curves of the commercial Pt plate for the HER (red line) and Pd PANs for the EGOR (blue line) in 1 M KOH.

Supplementary Note 7 and Supplementary Fig. 28 show that the potential window for the EGOR over Pd PNAs lies between the redox potential of $Na_{0.44}MnO_2$ and the onset potential of the HER. This suggests that a decoupled process can be achieved theoretically, with $Na_{0.44}MnO_2$ serving as the redox mediator and Pd PNAs acting as the EGOR electrocatalyst.

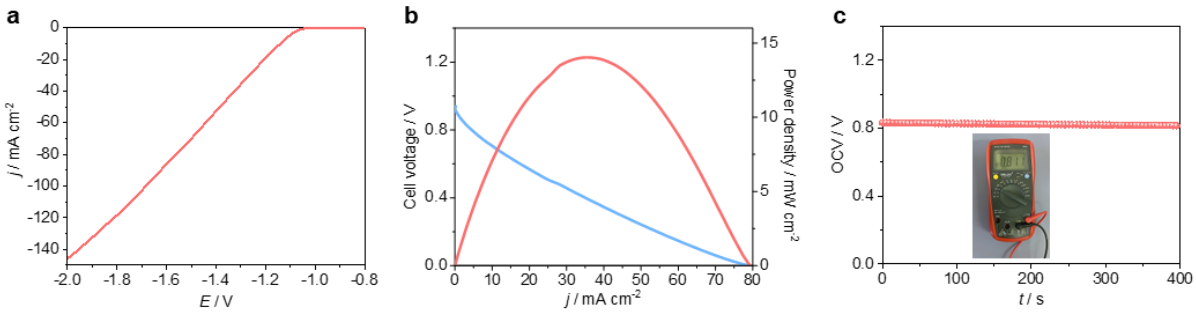

Supplementary Fig. 29 (a) LSV curve of the charging process, (b) discharging and power density curves, (**c**) OCV measurement for the decoupled cell using $Na_{0.44}MnO_2$ as the RM.

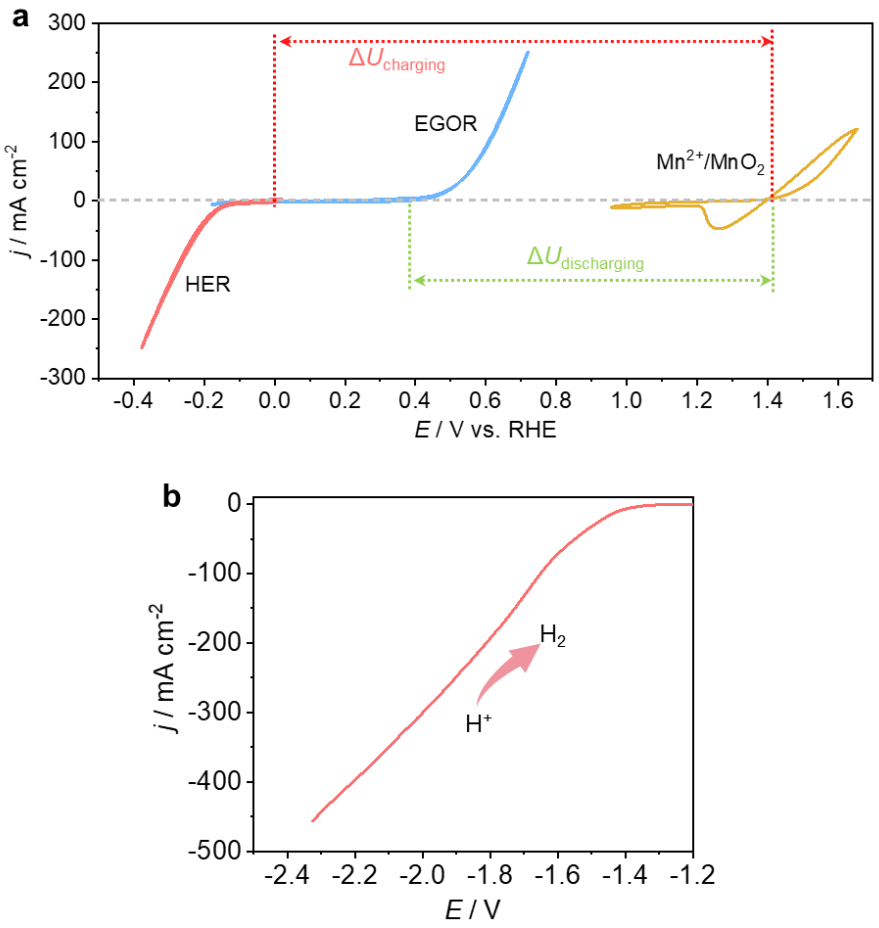

Supplementary Fig. 30 (a) CV curve of the Mn^{2+}/MnO_2 electrode (yellow line) and LSV curves of the commercial Pt plate for the HER (red line) and Pd PANs for the EGOR (blue line) in 1 M KOH. (b) LSV curve of the charging process.

Supplementary Table 3 Comparison of recently reported liquid fuel cells and electrocatalysis-battery hybrid systems.

Systems	Electrolyte (anode-cathode)	OCV (V)	Power density ($mW\ cm^{-2}$)	Ref
Zn-NO_3^-	Alkaline-Alkaline	1.49	8.91	[31]
Zn-NO_3^-	Alkaline-Alkaline	1.396	5.6	[32]
Zn-NO_3^-	Alkaline-Alkaline	1.38	19.4	[33]
Furfural–Co0.2Ni0.8(OH)2	Alkaline-Alkaline	1.29	107	[20]
Ethanol-NiOOH	Alkaline-Alkaline	0.95	11	[34]
N_2H_4-p-VHCF	Alkaline-Alkaline	0.5	9	[35]
Formaldehyde-NO_3^-	Alkaline-Alkaline	0.75	3.4	[36]
H_2-O_2	Alkaline-Acid	1.81	84.2	[37]
N_2H_4-H_2O (Acidic-alkaline asymmetric electrolyte)	Alkaline-Acid	1.14	34.8	[38]
Zn–H_2O	Alkaline–acid	1.25	80	[39]
EG-NCOOH	**Alkaline-Alkaline**	**0.89**	**14**	**This work**
EG-MnO_2	**Alkaline-Acid**	**1.785**	**133**	**This work**

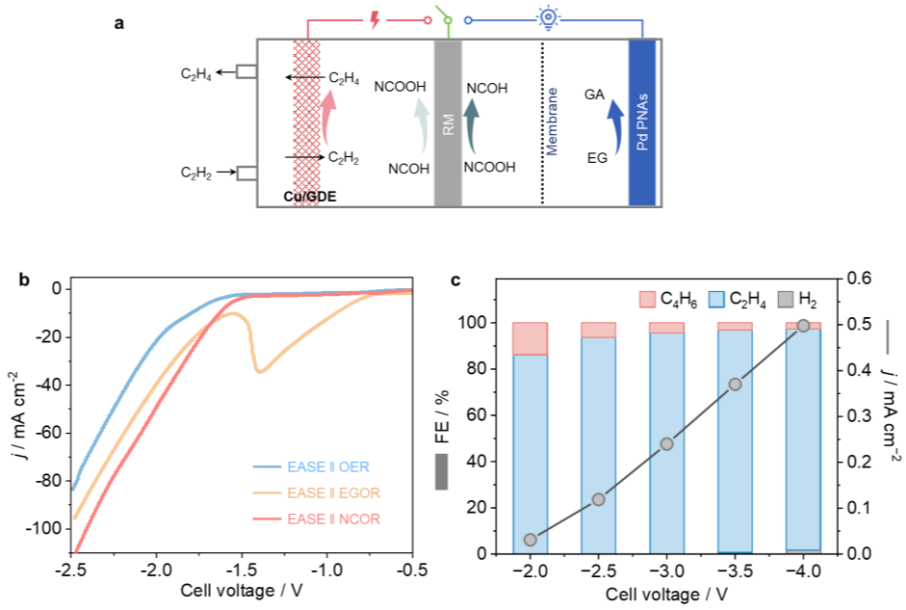

Supplementary Fig. 31 (a) Schematic diagram illustrating the decoupled flow cell of electrocatalytic semihydrogenation of coal-derived acetylene to ethylene (ESAE) paired with EGOR. (b) LSV curves for ESAE in the systems of ESAE || NCOR, ESAE || OER and ESAE || EGOR. (c) Cell voltage-dependent FE of obtained products and current density in Step 1.

Supplementary Note 8 We assembled a flow cell to verify the feasibility of a decoupling system to realize kinetically accelerated ESAE and simultaneous production of valuable GAs along with electricity storage/generation (Supplementary Fig. 31a). The low-coordination Cu nanoparticles on a gas diffusion electrode (Cu/GDE) reported in our previous work were selected as the ESAE electrode.[40]As demonstrated in Supplementary Fig. 31b, the LSV curves revealed that the ESAE ‖ NCOR system exhibited the fastest current density increase among the three systems, which is similar to the results demonstrated in Fig. 3a. In addition, a high ethylene FE of 97% at a current density of 500 mA cm-2 can be achieved under a low cell voltage in Step 1 (Supplementary Fig. 31c). When the NCOH was fully converted to NCOOH in Step 1, the reduction of NCOOH back to

NCOH and the oxidation of EG to GA released energy in Step 2 (discharging) when the switch was toggled. The results are the same as those in Fig. 4.

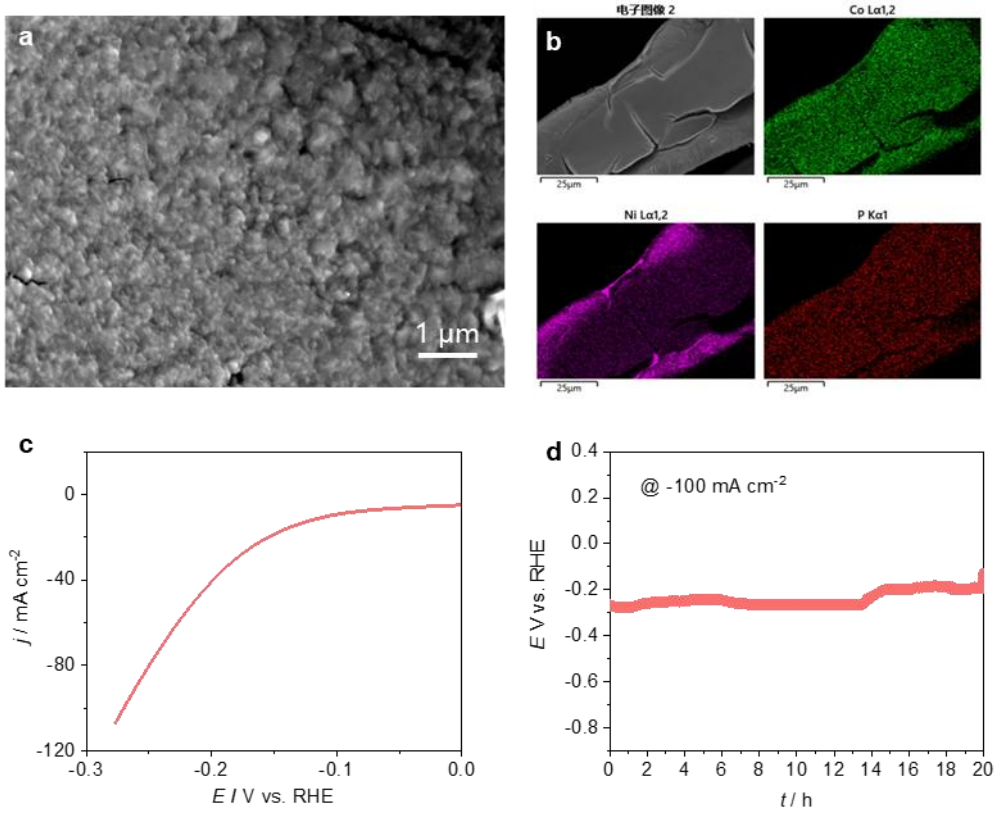

Supplementary Fig. 32 (**a**) SEM and (**b**) EDX elemental mapping images of NiCoP. (**c**) LSV curves of NiCoP in a 1 M KOH electrolyte. (**d**) Stability test of NiCoP for the HER at a current density of -100 mA cm^{-2}.

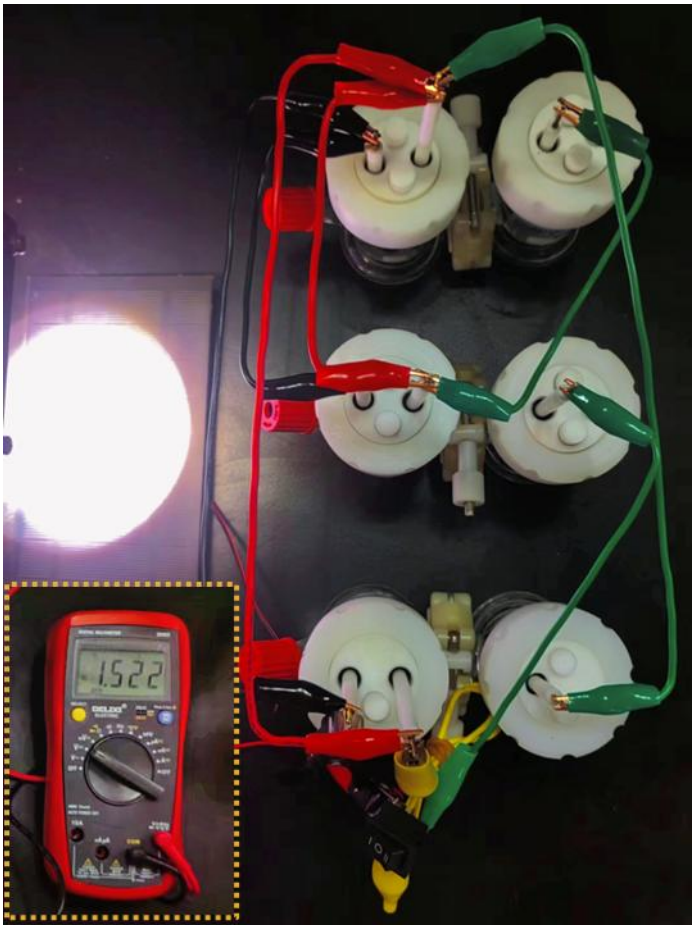

Supplementary Fig. 33 Photograph of three reaction cells linked in parallel powered by a photovoltaic cell (1.52 V).

Supplementary Fig. 34 Photographs showing the measurement of the volume of H_2 produced in the electrolysis cell via the drainage method.

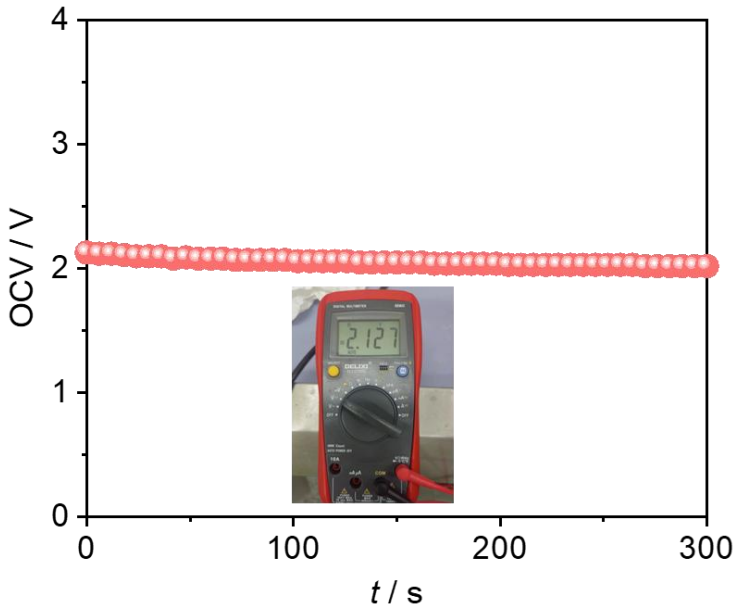

Supplementary Fig. 35 OCV measurement of three reactions configured in tandem for the discharging process.

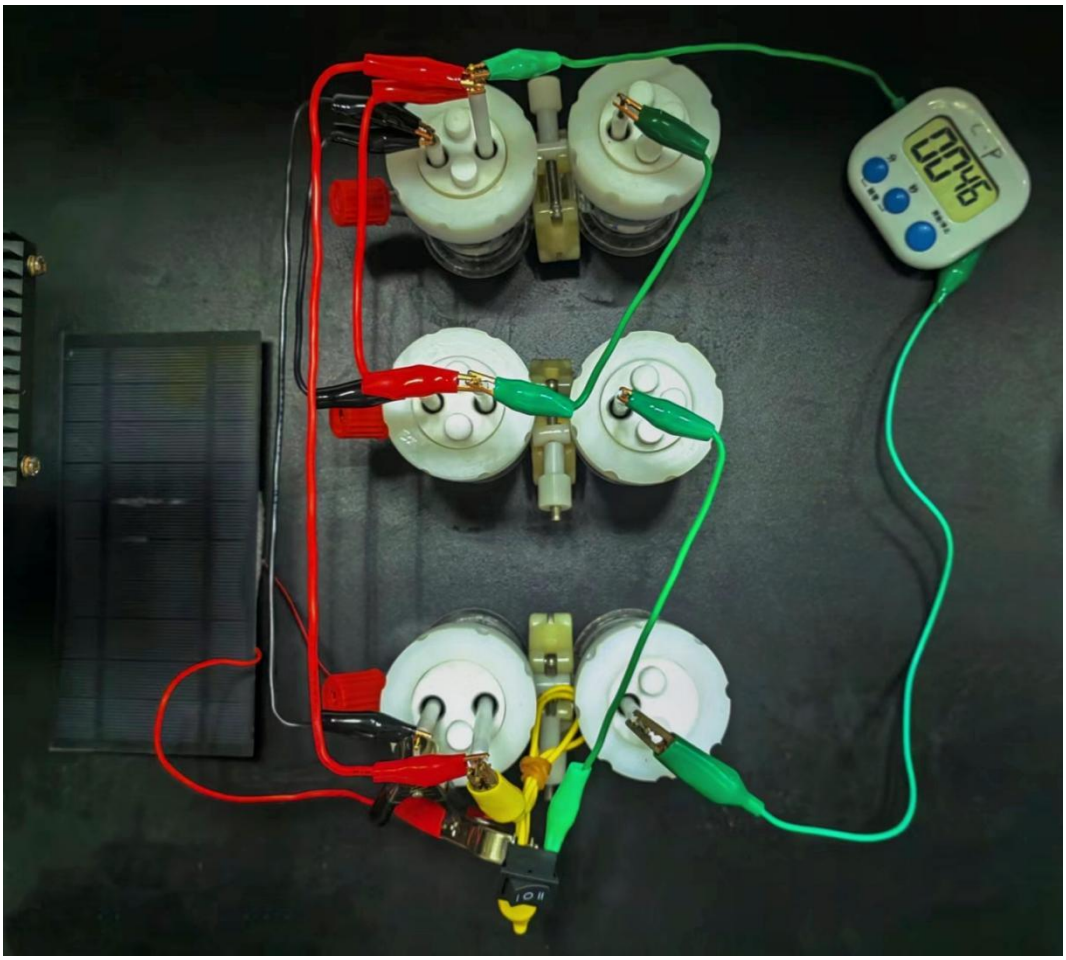

Supplementary Fig. 36 Photograph of three reactions configured in tandem to supply stable power for a timer.

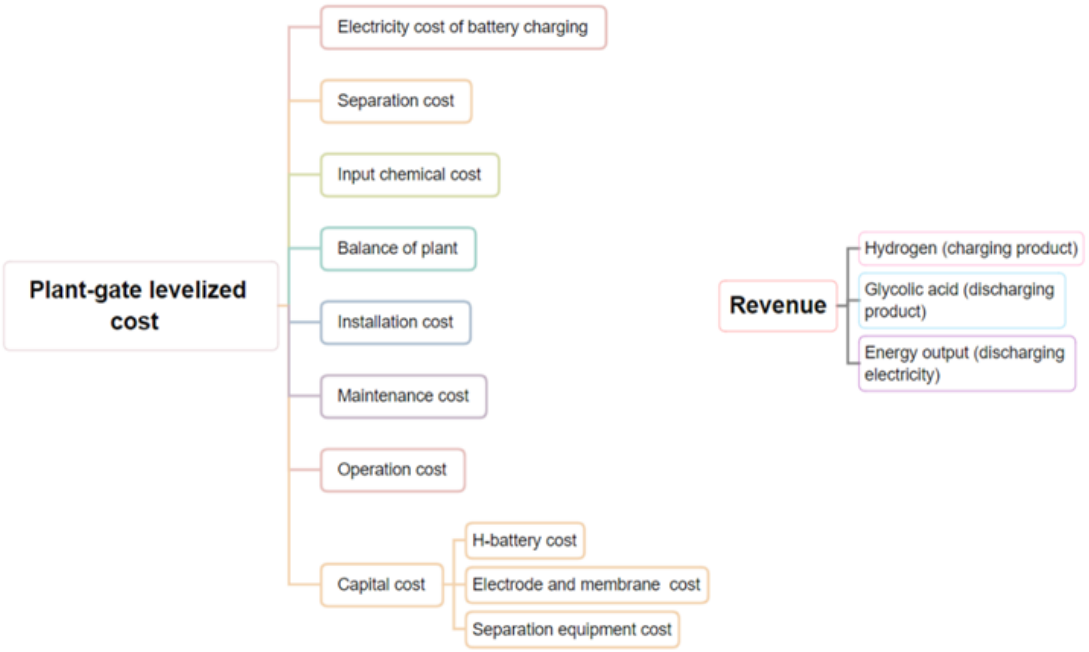

Supplementary Fig. 37 Model used for the technoeconomic analysis of H_2 and GA production via the decoupled system. The units are US$ per m^3 of liquid H_2. The detailed calculation process is shown in Supplementary Note 7.

Supplementary Note 9 Technoeconomic analysis

A preliminary technoeconomic analysis (TEA) of the biomass battery was conducted on the basis of a previously reported model with modifications[41–44]. The model made some reasonable assumptions to treat one ton of furfural per day for the charging process of the biomass battery:

Assumption #1: The electrolyzer plays an essential role in the electroreforming of P wastes, which is set at a cost of $10,000 per m^2. The electrode and membrane costs account for 5% of the flow battery cost. The separation equipment cost is 10% of the flow battery cost.

Assumption #2: The faradaic efficiency is 100% for H_2 and 85% for glycolic acid according to the battery charging and discharging results.

Assumption #3: The lifetime of the plant is assumed to be 10 years.

Assumption #4: The capacity factor depicts the operation time fraction of the plant on any given day and is assumed to be 0.8, which means that the plant will operate for 19.2 hours a day. Each charging and discharging process accounts for 50% (i.e., 9.6 hours), respectively.

Assumption #5: The coulombic efficiency of the battery is 97%, i.e., Qcharge = 97% × Qdischarge.

Assumption #6: The average charging and discharging voltages are assumed to be 1.65 V and 0.65 V, respectively.

Assumption #7: The separation cost is assumed to be 30% of the electricity cost. The electricity is assumed to be 0.1 $/kWh.

Assumption #8: Both the maintenance cost and operation cost are assumed to be 10% of the capital cost. The balance of plant and installation costs is calculated on the basis of the balance of the plant factor (0.2) and Lang factor (0.35) reported in the literature[42, 43].

Assumption #9: In terms of chemical cost, the prices of PET waste (0.39 $/kg), KOH (1.28 $/kg), and water ($2.24\times10^{-4}$ $/kg) are employed[42, 43]. The chemicals used for hydrogen production are listed in Supplementary Table S1.

Assumption #10: To calculate the potential profit, the market prices of products H_2 (2.79 $/kg) and glycolic acid (4.88 $/kg) are employed[42, 43]. The plant capacity for producing H_2 is 1 m^3 per day.

In this model, the plant-gate levelized cost includes 8 components: the electricity cost of battery charging, the separation cost, the capital cost, the balance of the plant, the installation cost, the maintenance cost, the operation cost, and the input chemical cost.

The detailed calculations of each component in the HER coupled with NiOR are as follows:

1. Electricity cost——50 mA cm^{-2}

We first calculate the total charge required for battery charging for 1 m ^{3}of H_2 per day on the basis of assumption #2.

$$\mathrm{Q_{charging}} = \frac{\text{Mass of H2O converted } \times \mathrm{F} \times \mathrm{n_{charging}}}{\mathrm{M_{H2O}} \times \mathrm{FE_{H2}}} = \frac{1.27 \times 10^6 \text{ g } \times \text{ 96485 C mol}^{-1} \times 2}{18 \text{ g mol}^{-1} \times 1}$$

$$= 1.36 \times 10^{10} \text{ C}$$

On the basis of assumption #5, the charges for the discharging process can be calculated:

$$Q_{discharge} = 97\% \times Q_{charge} = 97\% \times 1.36 \times 10^{10} \text{ C} = 1.32 \times 10^{10} \text{ C}$$

We then calculate the mass of the EG required for the discharging process:

$$m_{discharging} = \frac{Q_{discharging}}{F \times n_{discharge}} \times M_{EG} = \frac{1.32 \times 10^{10} \text{ C}}{96485 \text{ C mol}^{-1} \times 4} \times 62 \text{ g mol}^{-1} = 2.12 \times 10^3 \text{ kg}$$

We now calculate the current required for the battery charging process with a capacity factor of 0.8 on the basis of assumption #4.

$$I_{charging} = \frac{Q_{charge}}{t_{charge}} = \frac{1.36 \times 10^{10} \text{ C}}{9.6\ h \times 3600} = 3.94 \times 10^5 \text{ A}$$

The charging power can be calculated on the basis of assumption #6.

$$P_{charge} = I_{charging} \times U_{charging} = 3.94 \times 10^5 \text{ A} \times 1.39 \text{ V} = 548\ kW$$

The consumed electricity for battery charging can be calculated on the basis of Assumption #4:

$$\text{electricity of battery charging} = \mathrm{P_{charging}} \times \mathrm{t_{charging}} = 548\ kW \times 9.6\ h = 5260.8\ \mathrm{kWh}$$

Finally, the electricity cost of battery charging per day, normalized by the volume of KOH treated, can be calculated on the basis of Assumption #7:

$$\text{electricity cost of battery charging} = \frac{\text{electricity} \times \text{cost per kWh}}{\text{volume of } \mathrm{H_2} \text{ produced per day}}$$

$$= \frac{5260.8\ \mathrm{kWh} \times 0.1\ \$\ \mathrm{kwh^{-1}}}{1\ \mathrm{m^3}} = \$526.08 \text{ per } \mathrm{m^3} \text{ of } \mathrm{H_2}$$

2. Separation cost

The separation cost is assumed to be 30% of the electricity cost.

$$\text{separation cost} = 0.3 \times \$526.08 = \$157.82$$

3. Capital cost

The capital cost is composed of 3 components: battery cost, electrode and membrane cost, and separation equipment cost.

We first calculate the battery cost. On the basis of the current required and the assumed charging current density of 50 mA cm^{-2} (0.05 A cm^{-2}), we can calculate the area of the battery needed.

$$\text{Area of battery} = \frac{\text{Ichaging}}{\text{charing current density}} = \frac{3.94 \times 10^5\ \mathrm{A} \times 10^{-4}}{0.05\ \mathrm{A\ cm^{-2}}} = 788\ \mathrm{m^2}$$

The battery cost can now be calculated, and the estimate is \$10,000 per m^2 (assumption #1):

$$\text{Cost of battery} = 788\mathrm{m^2} \times \$10000 \text{ per } \mathrm{m^2} = 7.88 \times 10^6\$$$

The electrode and membrane costs and separation equipment costs are also calculated on the basis of assumption #1:

$$\text{Cost of electrode and membrance} = \text{cost of battery} \times 5\% = 7.88 \times 10^6\$ \times 5\% = 3.94 \times 10^5\$$$

$$\text{Cost of separation equipment} = \text{cost of battery} \times 10\% = 7.88 \times 10^6\$ \times \$10\% = 7.88 \times 10^5\$$$

Therefore, the capital cost normalized by the volume of H_2 produced per day can be calculated on the basis of assumption #3:

$$\text{Capital cost} = \frac{\text{cost of battery} + \text{cost of electrode and membrance} + \text{cost of separation equipment}}{\text{Lifetime of plant} \times V_{\text{total H2}} \text{ per day}}$$

$$= \frac{7.88 \times 10^6\$ + 3.94 \times 10^5\$ + 7.88 \times 10^5\$}{10 \text{ years} \times 365\text{days} \times 1 \text{ m}^3} = \$2.48 \times 10^3 \text{ per m}^3 \text{ of } H_2$$

4. Balance of a plant

Balance of a plant = capital cost $\times$ balance of plant factor = $\$2.48 \times 10^3 \times 0.2 = \$4.96 \times 10^2$

5. Maintenance cost

This value is assumed to be 10% of the capital costs (assumption #8).

Maintenance cost = capital cost $\times$ 10% = $\$2.48 \times 10^3 \times 0.1 = \$2.48 \times 10^2$

6. Operational cost

This value is assumed to be 10% of the capital costs (assumption #8).

Operation cost = capital cost $\times$ 10% = $\$2.48 \times 10^3 \times 0.1 = \$2.48 \times 10^2$

7. Input chemical cost

Chemicals require 2.5×10^3 kg of PET waste, 3.83×10^3 kg of KOH, and 6.97×10^4 kg of water, assuming that the feed concentration is ~ 1 M, where the costs of PET waste, KOH, and water are 0.39, 1.28, and 2.2 $\times 10^{-4}$ \$/kg, respectively. The calculated:

$$\text{Input chemical cost} = \frac{m_{\text{total PETwastes}} \times \text{price of PET wastes} + m_{\text{KOH}} \times \text{price of KOH} + m_{\text{water}} \times \text{price of water}}{V_{\text{total H2}}}$$

$$= \frac{2.12 \times 10^3 \text{ kg} \times 1.18 \times 0.39 \text{ \$ kg}^{-1} + 3.83 \times 10^3 \text{ kg} \times 1.28 \text{ \$ kg}^{-1} + 6.97 \times 10^4 \text{ kg} \times 0.00022\$ \text{ kg}^{-1}}{1 \text{ m}^3}$$

$$= \$5893.36 \text{ per m}^3 \text{ of } H_2$$

Total plant gate levelized cost:

Finally, the total cost can now be calculated by adding all 8 components:

Total cost = \$526.08 + \$157.82 + \$2480+ \$496+ \$248 + \$248+ \$5893.36 = \$10049.26 per m^3 of H_2

Revenue:

The potential revenue contains the profit from H_2, the GA and the electricity output. We calculate the mass of H_2 and the GA produced per day on the basis of Assumption #2:

$$m_{H2} = 70.8\ kg$$

$$m_{\mathrm{GA}} = \frac{Q_{\mathrm{discharge}} \times FE\ of\ GA}{F \times n_{\mathrm{charge}}} \times M_{\mathrm{GA}} = \frac{1.32 \times 10^{10}\ C \times 0.85}{4 \times 96485\ C\ \mathrm{mol}^{-1}} \times 76.05\ \mathrm{g\ mol}^{-1} = 2.21 \times 10^{3}\ \mathrm{kg}$$

Therefore, the revenue from chemical production normalized to one cubic meter of H_2 can be calculated.

$$Revenue\ from\ chemical\ production = \frac{m_{H2} \times price\ of\ H_2 + m_{GA} \times price\ of\ GA}{V_{H2}}$$

$$= \frac{70.8\ kg \times 2.79\ \$\ kg^{-1} + 2.21 \times 10^{3}\ kg \times 4.88\ \$\ kg^{-1}}{1\ m^3}$$

$$= \$10982.33\ per\ m^3\ of\ H_2$$

The electricity output (kWh) was calculated on the basis of assumption #6:Electricity output = $\mathrm{Q_{discharge}} \times \mathrm{U_{dischage}} = 1.32 \times 10^{10}\mathrm{C} \times 0.65\ \mathrm{V} = 2380\ \mathrm{kWh}$

The electricity output normalized to one cubic meter of H_2 can be calculated.

$$\text{Electricity output per m}^3\text{ of H}_2 = \frac{\text{Electricity output}}{\mathrm{V_{H2}}} = \frac{2380\ \mathrm{kWh}}{1\ \mathrm{m}^3} = 2380\ \text{per m}^3\text{ of H}_2$$

The revenue from electricity output can be calculated on the basis of Assumption #7:

$$\text{Revenue from electricity output} = \text{Electrcity output per ton of KOH} \times \text{electricity price}$$

$$= 2380\ \mathrm{kWh} \times 0.1\ \$\ \mathrm{kWh}^{-1} = \$238\ \text{per m}^3\text{ of H}_2$$

Therefore, the total revenue can be obtained.

$$\text{Total revenue} = \text{Revenue from chemical production} + \text{Revenue from electricity output}$$

$$= \$10982.33 + \$238 = \$11220.33 \text{ per m}^3 \text{ of } H_2$$

Net profit:

The net profit can be obtained.

Total revenue = Total cost − Total revenue = $\$11220.33 - \$10049.26 = \$1171.07$ per m^3 of H_2

1. Electricity cost——100 mA cm^{-2}

We first calculate the total charge required for battery charging for 1 m^3 of H_2 per day on the basis of assumption #2.

$$Q_{\text{charging}} = \frac{\text{Mass of H2O converted} \times F \times n_{\text{charging}}}{M_{H2O} \times FE_{H2}} = \frac{1.27 \times 10^6 \text{ g} \times 96485 \text{ C mol}^{-1} \times 2}{18 \text{ g mol}^{-1} \times 1}$$

$$= 1.36 \times 10^{10} \text{ C}$$

On the basis of assumption #5, the charges for the discharging process can be calculated:

$$Q_{\text{discharge}} = 97\% \times Q_{\text{charge}} = 97\% \times 1.36 \times 10^{10} \text{ C} = 1.32 \times 10^{10} \text{ C}$$

We then calculate the mass of the EG required for the discharging process:

$$m_{\text{discharging}} = \frac{Q_{\text{discharging}}}{F \times n_{\text{discharge}}} \times M_{EG} = \frac{1.32 \times 10^{10} \text{ C}}{96485 \text{ C mol}^{-1} \times 4} \times 62 \text{ g mol}^{-1} = 2.12 \times 10^3 \text{ kg}$$

We now calculate the current required for the battery charging process with a capacity factor of 0.8 on the basis of assumption #4.

$$I_{charging} = \frac{Q_{charge}}{t_{charge}} = \frac{1.36 \times 10^{10} \text{ C}}{9.6\ h \times 3600} = 3.94 \times 10^5 \text{ A}$$

The charging power can be calculated on the basis of assumption #6.

$$P_{charge} = I_{charging} \times U_{charging} = 3.94 \times 10^5 \text{ A} \times 1.52 \text{ V} = 599\ kW$$

The consumed electricity for battery charging can be calculated on the basis of Assumption #4:

$$\text{electricity of battery charging} = \text{P}_{\text{charging}} \times \text{t}_{\text{charging}} = 599\ kW \times 9.6\ h = 5750.4 \text{ kWh}$$

Finally, the electricity cost of battery charging per day, normalized by the volume of KOH treated, can be calculated on the basis of assumption #7:

$$\text{electricity cost of battery charging} = \frac{\text{electricity} \times \text{cost per kWh}}{\text{volume of } \text{H}_2 \text{ produced per day}}$$
$$= \frac{5750.4 \text{ kWh} \times 0.1 \text{ \$ kwh}^{-1}}{1 \text{ m}^3} = \$575.04 \text{ per m}^3 \text{ of H}_2$$

2. Separation cost

The separation cost is assumed to be 30% of the electricity cost.

$$\text{separation cost} = 0.3 \times \$575.04 = \$172.51$$

3. Capital cost

The capital cost is composed of 3 components: battery cost, electrode and membrane cost, and separation equipment cost.

We first calculate the battery cost. On the basis of the current required and the assumed charging current density of 100 mA cm^{-2} (0.1 A cm^{-2}), we can calculate the area of the battery needed.

$$\text{Area of battery} = \frac{\text{Ichaging}}{\text{charing current density}} = \frac{3.94 \times 10^5 \text{ A} \times 10^{-4}}{0.1 \text{ A cm}^{-2}} = 394 \text{ m}^2$$

The battery cost can now be calculated, and the estimate is \$10,000 per m^2 (assumption #1):

$$\text{Cost of battery} = 394 \text{ m}^2 \times \$10000 \text{ per m}^2 = 3.94 \times 10^6 \$$$

The electrode and membrane costs and separation equipment costs are also calculated on the basis of assumption #1:

$$\text{Cost of electrode and membrance} = \text{cost of battery} \times 5\% = 3.94 \times 10^6 \$ \times 5\% = 1.97 \times 10^5 \$$$

$$\text{Cost of separation equipment} = \text{cost of battery} \times 10\% = 3.94 \times 10^6\$ \times \$10\% = 3.94 \times 10^5\$$$

Therefore, the capital cost normalized by the volume of H_2 produced per day can be calculated on the basis of assumption #3:

$$\text{Capital cost} = \frac{\text{cost of battery} + \text{cost of electrode and membrance} + \text{cost of separation equipment}}{\text{Lifetime of plant} \times \text{V}_{\text{total H2}} \text{ per day}}$$

$$= \frac{3.94 \times 10^6\$ + 1.97 \times 10^5\$ + 3.94 \times 10^5\$}{10 \text{ years} \times 365\text{days} \times 1 \text{ m}^3} = \$1.24 \times 10^3 \text{ per m}^3 \text{ of H}_2$$

4. Balance of a plant

Balance of a plant = capital cost $\times$ balance of plant factor = $\$1.24 \times 10^3 \times 0.2 = \$2.48 \times 10^2$

5. Maintenance cost

This value is assumed to be 10% of the capital costs (assumption #8).

Maintenance cost = capital cost $\times 10\% = \$1.24 \times 10^3 \times 0.1 = \$1.24 \times 10^2$

6. Operational cost

This value is assumed to be 10% of the capital costs (assumption #8).

Operation cost = capital cost $\times 10\% = \$1.24 \times 10^3 \times 0.1 = \$1.24 \times 10^2$

7. Input chemical cost

Chemicals require 2.5×10^3 kg of PET waste, 3.83×10^3 kg of KOH, and 6.97×10^4kg of water, assuming that the feed concentration is ~ 1 M, where the costs of PET waste, KOH, and water are 0.39, 1.28, and 2.2×10^{-4} \$/kg, respectively. The input chemical cost normalized by the volume of H_2 produced can be calculated as follows:

Input chemical cost

$$= \frac{m_{\text{total PETwastes}} \times \text{price of PET wastes} + m_{KOH} \times \text{price of KOH} + m_{water} \times \text{price of water}}{V_{\text{total H2}}}$$

$$= \frac{2.12 \times 10^3 \text{ kg} \times 1.18 \times 0.39 \$\,\text{kg}^{-1} + 3.83 \times 10^3 \text{ kg} \times 1.28 \$\,\text{kg}^{-1} + 6.97 \times 10^4 \text{ kg} \times 0.00022 \$\,\text{kg}^{-1}}{1 \text{ m}^3}$$

$= \$5893.36 \text{per m}^3 \text{ of } H_2$

Total plant gate levelized cost:

Finally, the total cost can now be calculated by adding all 8 components:

Total cost = \$575.04 + \$172.51 + \$1240+ \$248+ \$124+ \$124+ \$5893.36 = \$8376.91 per m^3 of H_2

Revenue: (same as 50 mA cm^{-2})

1. Electricity cost——200 mA cm^{-2}

We first calculate the total charge required for battery charging for 1 m^3 of H_2 per day on the basis of assumption #2.

$$Q_{\text{charging}} = \frac{\text{Mass of H2O converted} \times F \times n_{\text{charging}}}{M_{H2O} \times FE_{H2}} = \frac{1.27 \times 10^6 \text{ g} \times 96485 \text{ C mol}^{-1} \times 2}{18 \text{ g mol}^{-1} \times 1}$$

$$= 1.36 \times 10^{10} \text{ C}$$

On the basis of assumption #5, the charges for the discharging process can be calculated:

$$Q_{\text{discharge}} = 97\% \times Q_{\text{charge}} = 97\% \times 1.36 \times 10^{10} \text{ C} = 1.32 \times 10^{10} \text{ C}$$

We then calculate the mass of the EG required for the discharging process:

$$m_{\text{discharging}} = \frac{Q_{\text{discharging}}}{F \times n_{\text{discharge}}} \times M_{\text{EG}} = \frac{1.32 \times 10^{10} \text{ C}}{96485 \text{ C mol}^{-1} \times 4} \times 62 \text{ g mol}^{-1} = 2.12 \times 10^3 \text{ kg}$$

We now calculate the current required for the battery charging process with a capacity factor of 0.8 on the basis of assumption #4.

$$I_{\text{charging}} = \frac{Q_{\text{charge}}}{t_{\text{charge}}} = \frac{1.36 \times 10^{10}\ \text{C}}{9.6\ h \times 3600} = 3.94 \times 10^{5}\ \text{A}$$

The charging power can be calculated on the basis of assumption #6.

$$P_{\text{charge}} = I_{\text{charging}} \times U_{\text{charging}} = 3.94 \times 10^{5}\ \text{A} \times 1.76\ \text{V} = 693\ kW$$

The consumed electricity for battery charging can be calculated on the basis of Assumption #4:

$$\text{electricity of battery charging} = \text{P}_{\text{charging}} \times \text{t}_{\text{charging}} = 693\ kW \times 9.6\ h = 6652.8\ \text{kWh}$$

Finally, the electricity cost of battery charging per day, normalized by the volume of KOH treated, can be calculated on the basis of Assumption #7:

$$\text{electricity cost of battery charging} = \frac{\text{electricity} \times \text{cost per kWh}}{\text{volume of } \text{H}_2 \text{ produced per day}}$$
$$= \frac{6652.8\ \text{kWh} \times 0.1\ \$\ \text{kwh}^{-1}}{1\ \text{m}^3} = \$665.28\ \text{per m}^3\ \text{of H}_2$$

2. Separation cost

The separation cost is assumed to be 30% of the electricity cost.

$$\text{separation cost} = 0.3 \times \$665.28 = \$199.58$$

3. Capital cost

The capital cost is composed of 3 components: battery cost, electrode and membrane cost, and separation equipment cost.

We first calculate the battery cost. On the basis of the current required and the assumed charging current density of 200 mA cm^{-2} (0.2 A cm^{-2}), we can calculate the area of the battery needed.

$$\text{Area of battery} = \frac{\text{Ichaging}}{\text{charing current density}} = \frac{3.94 \times 10^{5}\ \text{A} \times 10^{-4}}{0.2\ \text{A cm}^{-2}} = 197\ \text{m}^2$$

The battery cost can now be calculated, and the estimate is \$10,000 per m^2 (assumption #1):

$$\text{Cost of battery} = 197\ \text{m}^2 \times \$10000\ \text{per m}^2 = 1.97 \times 10^{6}\$$$

The electrode and membrane costs and separation equipment costs are also calculated on the basis of assumption #1:

$$\text{Cost of electrode and membrance} = \text{cost of battery} \times 5\% = 1.97 \times 10^6\$ \times 5\% = 9.85 \times 10^4\$$$

$$\text{Cost of separation equipment} = \text{cost of battery} \times 10\% = 1.97 \times 10^6\$ \times \$10\% = 1.97 \times 10^5\$$$

Therefore, the capital cost normalized by the volume of H_2 produced per day can be calculated on the basis of assumption #3:

$$\text{Capital cost} = \frac{\text{cost of battery} + \text{cost of electrode and membrance} + \text{cost of separation equipment}}{\text{Lifetime of plant} \times V_{\text{total H2}} \text{ per day}}$$

$$= \frac{1.97 \times 10^6\$ + 9.85 \times 10^4\$ + 1.97 \times 10^5\$}{10 \text{ years} \times 365\text{days} \times 1 \text{ m}^3} = \$6.21 \times 10^2 \text{ per m}^3 \text{ of } H_2$$

4. Balance of a plant

Balance of plant = capital cost $\times$ balance of plant factor = $\$6.21 \times 10^2 \times 0.2 = 1.24 \times 10^2$

5. Maintenance cost

This value is assumed to be 10% of the capital costs (assumption #8).

Maintenance cost = capital cost $\times$ 10% = $\$6.21 \times 10^2 \times 0.1 = \$0.62 \times 10^2$

6. Operational cost

This value is assumed to be 10% of the capital costs (assumption #8).

Operation cost = capital cost $\times$ 10% = $\$6.21 \times 10^2 \times 0.1 = \$0.62 \times 10^2$

7. Input chemical cost

Chemicals require 2.5×10^3 kg of PET waste, 3.83×10^3 kg of KOH, and 6.97×10^4 kg of water, assuming that the feed concentration is ~ 1 M, where the costs of PET waste, KOH, and

water are 0.39, 1.28, and 2.2 $\times 10^{-4}$ \$/kg, respectively. The input chemical cost normalized by the volume of H_2 produced can be calculated as follows:

$$\text{Input chemical cost}$$

$$= \frac{m_{\text{total PETwastes}} \times \text{price of PET wastes} + m_{KOH} \times \text{price of KOH} + m_{water} \times \text{price of water}}{V_{\text{total H2}}}$$

$$= \frac{2.12 \times 10^3 \text{ kg} \times 1.18 \times 0.39 \text{ \$ kg}^{-1} + 3.83 \times 10^3 \text{ kg} \times 1.28 \text{ \$ kg}^{-1} + 6.97 \times 10^4 \text{ kg} \times 0.00022 \text{\$ kg}^{-1}}{1 \text{ m}^3}$$

$$= \$5893.36 \text{ per m}^3 \text{ of } H_2$$

Total plant gate levelized cost:

Finally, the total cost can now be calculated by adding all 8 components:

Total cost = \$665.28 + \$199.58 + \$621+ \$124+ \$62 + \$62+ \$5893.36 = \$7627.22 per m ^{3}of H_2

Revenue: (same as 50 mA cm^{-2})

Supplementary Note 10 Chemicals

Cobalt nitrate ($Co(NO_3)_2 \cdot 6H_2O$, 99.0%), nickel nitrate ($Ni(NO_3)_2 \cdot 6H_2O$, 99.0%), and sodium hypophosphate (NaH_2PO_2, 99.0%) were purchased from Aladdin Ltd. (Shanghai, China). Ethylene glycol ($HOCH_2CH_2OH$, 99.9%) was purchased from Macklin Biochemical Technology Co., Ltd. (Shanghai, China). Sodium tetrachloropalladate (II) (Na_2PdCl_4, 99.0%) was purchased from Bide Pharmatech Ltd. (Shanghai, China). Potassium hydroxide (KOH, 99.0%) was purchased from Sinopharm Chemical Reagent Co., Ltd. (Shanghai, China). 5% H_2/Ar was purchased from Xiangyun Industry and Trade Co., Ltd. (Wuhan, China).

References

1. Xu Y, *et al.* Methanol electroreforming coupled to green hydrogen production over bifunctional NiIr-based metal-organic framework nanosheet arrays. *Applied Catalysis B: Environmental* **300**, 120753 (2022).
2. Du R, *et al.* Optimized Electrodeposition of Ni_2O_3 on Carbon Paper for Enhanced Electrocatalytic Oxidation of Ethanol. *ACS Omega* **9**, 30404-30414 (2024).
3. Fu H, *et al.* Surface-Regulated Platinum–Copper Nanoframes in Electrochemical Reforming of Ethanol for Efficient Hydrogen Production. *ACS Catalysis* **12**, 11402-11411 (2022).
4. Liu L, He Y, Ma D-D, Wu X-T, Zhu Q-L. Directional editing of self-supported nanoarray electrode for adaptive paired-electrolysis. *Journal of Colloid and Interface Science* **640**, 423-433 (2023).
5. Si D, Xiong B, Chen L, Shi J. Highly selective and efficient electrocatalytic synthesis of glycolic acid in coupling with hydrogen evolution. *Chem Catalysis* **1**, 941-955 (2021).
6. Ma L, *et al.* Promoting Electrocatalytic Glycerol C─ C Bond Cleavage to Formate Coupled with H_2 Production Over a $Cu_xNi_{2-x}P$ Catalyst. *Advanced Energy Materials* **14**, 2401061 (2024).
7. Yan Y, *et al.* Electrocatalytic Upcycling of Biomass and Plastic Wastes to Biodegradable Polymer Monomers and Hydrogen Fuel at High Current Densities. *Journal of the American Chemical Society* **145**, 6144-6155 (2023).
8. Shanker GS, *et al.* Regulation of Catalyst Immediate Environment Enables Acidic Electrochemical Benzyl Alcohol Oxidation to Benzaldehyde. *ACS Catalysis* **14**, 5654-5661 (2024).
9. Li Z, *et al.* Alcohols electrooxidation coupled with H2 production at high current densities promoted by a cooperative catalyst. *Nature Communications* **13**, 147 (2022).
10. Li M, Wang T, Zhao W, Wang S, Zou Y. A Pair-Electrosynthesis for Formate at Ultra-Low Voltage Via Coupling of CO_2 Reduction and Formaldehyde Oxidation. *Nano-Micro Letters* **14**, 211 (2022).
11. Begildayeva T, *et al.* Sustainable furfural biomass feedstocks electrooxidation toward value-added furoic acid with energy-saving H_2 fuel production using Pt-decorated Co_3O_4 nanospheres. *Energy Environmental Materials* **7**, e12563 (2024).
12. Song Y, *et al.* Ultrathin layered double hydroxides nanosheets array towards efficient electrooxidation of 5-hydroxymethylfurfural coupled with hydrogen generation. *Applied Catalysis B: Environmental* **299**, 120669 (2021).

13. Huang Y, Chong X, Liu C, Liang Y, Zhang BJAC. Boosting hydrogen production by anodic oxidation of primary amines over a NiSe nanorod electrode. *Angewandte Chemie* **130**, 13347-13350 (2018).
14. Huang C, Huang Y, Liu C, Yu Y, Zhang BJAC. Integrating hydrogen production with aqueous selective semi-dehydrogenation of tetrahydroisoquinolines over a Ni_2P bifunctional electrode. *Angewandte Chemie* **131**, 12142-12145 (2019).
15. Yang D, Yang L, Zhong L, Yu X, Feng L. Urea electro-oxidation efficiently catalyzed by nickel-molybdenum oxide nanorods. *Electrochimica Acta* **295**, 524-531 (2019).
16. Liu W-J, *et al.* Efficient electrochemical production of glucaric acid and H_2 via glucose electrolysis. *Nature Communications* **11**, 265 (2020).
17. Li D, *et al.* Coupling overall water splitting and biomass oxidation via Fe-doped Ni_2P@C nanosheets at large current density. *Applied Catalysis B: Environment and Energy* **307**, 121170 (2022).
18. Chen Z-J, *et al.* Acidic enol electrooxidation-coupled hydrogen production with ampere-level current density. *Nature Communications* **14**, 4210 (2023).
19. Wang W, *et al.* Vacancy-Rich $Ni(OH)_2$ Drives the Electrooxidation of Amino C− N Bonds to Nitrile C≡ N Bonds. *Angewandte Chemie* **132**, 17122-17129 (2020).
20. Li J, *et al.* Rechargeable Biomass Battery for Electricity Storage/generation and Concurrent Valuable Chemicals Production. *Angew Chem Int Ed* **62**, e202304852 (2023).
21. Shi K, Si D, Teng X, Chen L, Shi J. Pd/$NiMoO_4$/NF electrocatalysts for the efficient and ultra-stable synthesis and electrolyte-assisted extraction of glycolate. *Nat Commun* **15**, 2899 (2024).
22. Liu X, *et al.* Electro-Reforming of PET Plastic to C2 Chemicals with Concurrent Generation of Hydrogen and Electric Energy. *ACS Catal* **14**, 5366-5376 (2024).
23. Ren T, *et al.* Electrochemical Co-Production of Ammonia and Biodegradable Polymer Monomer Glycolic Acid via the Co-Electrolysis of Nitrate Wastewater and Waste Plastic. *ACS Catal* **13**, 10394-10404 (2023).
24. Si D, Xiong B, Chen L, Shi J. Highly selective and efficient electrocatalytic synthesis of glycolic acid in coupling with hydrogen evolution. *Chem Catal* **1**, 941–955 (2021).
25. Du M, *et al.* Electrochemical Production of Glycolate Fuelled By Polyethylene Terephthalate Plastics with Improved Techno-Economics. *Small* **19**, 2303693 (2023).
26. Liu F, Gao X, Shi R, Guo Z, Tse ECM, Chen Y. Concerted and Selective Electrooxidation of Polyethylene-Terephthalate-Derived Alcohol to Glycolic Acid at an Industry-Level Current Density over a Pd−Ni(OH)2 Catalyst. *Angew Chem Int Ed* **62**, e202300094 (2023).

27. Yan Y, *et al.* Electrocatalytic Upcycling of Biomass and Plastic Wastes to Biodegradable Polymer Monomers and Hydrogen Fuel at High Current Densities. *J Am Chem Soc* **145**, 6144-6155 (2023).
28. Bhattacharjee S, Andrei V, Pornrungroj C, Rahaman M, Pichler CM, Reisner E. Reforming of Soluble Biomass and Plastic Derived Waste Using a Bias-Free Cu30Pd70|Perovskite|Pt Photoelectrochemical Device. *Adv Funct Mater* **32**, 2109313 (2022).
29. Liu K, *et al.* Energy-Saving Hydrogen Production by Seawater Splitting Coupled with PET Plastic Upcycling. *Adv Energy Mater* **14**, 2304065 (2024).
30. Yang H, *et al.* A universal ligand mediated method for large scale synthesis of transition metal single atom catalysts. *Nature Communications* **10**, 10 (2019).
31. Guan J, Cai L, Li W, Zhou H, Huang Y. Boosting nitrate electroreduction to ammonia on atomic Ru-Co pair sites in hollow spinels. *Appl. Catal. B: Environ. & Energy* **358**, 124387 (2024).
32. Jin T, *et al.* Mechanochemical-tuning size dependence of iridium single atom and nanocluster toward highly selective ammonium production. *Chem Catal* **3**, 100477 (2023).
33. Wan Y, *et al.* Interfacial Water Regulation for Nitrate Electroreduction to Ammonia at Ultralow Overpotentials. *Adv Mater* **38**, 2417696 (2025).
34. Ma Y, Dong X, Wang R, Bin D, Wang Y, Xia Y. Combining water reduction and liquid fuel oxidization by nickel hydroxide for flexible hydrogen production. *Energy Storage Mater* **11**, 260-266 (2018).
35. Lv F, *et al.* Decoupled electrolysis for hydrogen production and hydrazine oxidation via high-capacity and stable pre-protonated vanadium hexacyanoferrate. *Nat Commun* **15**, 1339 (2024).
36. An S, *et al.* Multi-Functional Formaldehyde-Nitrate Batteries for Wastewater Refining, Electricity Generation, and Production of Ammonia and Formate. *Angew Chem Int Ed* **63**, e202318989 (2024).
37. Shi L, *et al.* Stable and High-performance Flow H_2-O_2 Fuel Cells with Coupled Acidic Oxygen Reduction and Alkaline Hydrogen Oxidation Reactions. *Adv Mater* **36**, 2314077 (2024).
38. Sun F, He D, Yang K, Qiu J, Wang Z. Hydrogen Production and Water Desalination with On-demand Electricity Output Enabled by Electrochemical Neutralization Chemistry. *Angew Chem Int Ed* **61**, e202203929 (2022).
39. Cai P, Li Y, Wang G, Wen Z. Alkaline–Acid Zn–H_2O Fuel Cell for the Simultaneous Generation of Hydrogen and Electricity. **57**, 3910-3915 (2018).

40. Zhao B-H, *et al.* Economically viable electrocatalytic ethylene production with high yield and selectivity. *Nature Sustainability* **6**, 827-837 (2023).
41. Zhou H, *et al.* Electrocatalytic upcycling of polyethylene terephthalate to commodity chemicals and H2 fuel. *Nature Communications* **12**, 4679 (2021).
42. Lum Y, *et al.* Tuning OH binding energy enables selective electrochemical oxidation of ethylene to ethylene glycol. *Nature Catalysis* **3**, 14-22 (2020).
43. Leow WR, *et al.* Chloride-mediated selective electrosynthesis of ethylene and propylene oxides at high current density. **368**, 1228-1233 (2020).
44. Li J, *et al.* Rechargeable Biomass Battery for Electricity Storage/generation and Concurrent Valuable Chemicals Production. **62**, e202304852 (2023).